Journal of
Materials Chemistry A

PERSPECTIVE

View Article Online
View Journal | View Issue

Cite this: *J. Mater. Chem. A*, 2024, **12**, 25696

# Revisiting the ionic conductivity of solid oxide electrolytes: a technical review†

Danil E. Matkin,[ab] Inna A. Starostina,*[ab] Muhammad Bilal Hanif[cd] and Dmitry A. Medvedev*[ab]

Received 4th June 2024
Accepted 2nd September 2024

DOI: 10.1039/d4ta03852e

rsc.li/materials-a

Oxygen-ionic and proton-conducting oxides are an important class of functional materials for their applications as electrolytes in various high-temperature electrochemical cells, including solid oxide fuel cells (SOFCs), solid oxide electrolysis cells (SOECs), proton ceramic fuel cells (PCFCs), and proton ceramic electrolysis cells (PCECs). The electrolyte, as a heart of these cells, must meet a number of stringent requirements, among which its ionic conductivity is one of the most important parameters determining the possible applications in electrochemical devices and operating temperatures. In the present work, we provide a comparative analysis of the ionic conductivity for several classical electrolyte classes, such as stabilized/doped $ZrO_2$, $CeO_2$, $LaGaO_3$, $BaCeO_3$, $BaZrO_3$, and $Ba(Ce,Zr)O_3$. This analysis provides possible windows of conductivity variation and potential (common and specific) factors responsible for conductivity differences for the same materials and measurement conditions. In addition, the ionic conductivity is discussed not only for massive ceramic electrolytes, but also for their thin-film form in SOFCs/PCFCs or SOECs/PCECs. As a result, the transport properties of the state-of-the-art electrolytes have been revised and compared to show which system prevails over the other under different experimental conditions. Therefore, this technical review can be used as a reference source to provide useful information on oxygen-ionic and protonic conductivity for the most popular solid oxide electrolytes.

## 1 Introduction

Solid oxide electrochemical devices operating at elevated temperatures (above 400 °C) provide a promising basis for various energy conversion processes involving hydrogen, oxygen, carbon, and nitrogen-containing compounds.[1–5] Such a wide variety of electrochemical processes allows these devices to be used to meet many of the challenges facing a "green" future related to the development of hydrogen energy, renewable energy, and low-carbon technologies. For this reason, solid oxide fuel cells (SOFCs) and solid oxide electrolysis cells (SOECs) are considered as the most promising alternatives among other representatives of fuel and electrolysis cells.[6–10] Significant advancements have been made in the research and development of SOFC and SOEC stacks, with applications spanning portable (from several watts) and stationary (from several to hundreds of kilowatts) energy production and storage.[4,11–14] Furthermore, these prototypes have undergone rigorous testing for more than 20 000 hours,[15–19] providing compelling evidence of their long-term reliability.

The unit SOFC and SOEC cells are multilayered "sandwich-like" structures comprising a specific number of functional materials in contact with each other, which are then repeated sequentially.[20–22] Among the functional materials, an electrolyte is considered as a heart of solid oxide electrochemical cells performing a multitude of functions in the realization of electrochemical processes related to the conversion of different types of energy. It is well known that conventional SOFCs and SOECs are based on zirconia electrolytes (for example, yttria- or scandia-stabilized zirconia) as representative oxygen-ionic materials. Their ionic conductivity reaches acceptable levels at elevated temperatures (800–1000 °C), which explains why the related SOFCs and SOECs yield high performance under such severe conditions. Nevertheless, elevated operating temperatures result in rapid performance degradation, which is attributed to different factors, including chemical interactions and microstructural changes.[23–28] To address these issues, two commonly employed strategies have been utilized as a means of enhancing performance at reduced temperatures. The first

---

[a] *Laboratory of Electrochemical Devices Based on Solid Oxide Proton Electrolytes, Institute of High-Temperature Electrochemistry, 620066 Yekaterinburg, Russia. E-mail: fair696@yandex.ru; dmitrymedv@mail.ru*

[b] *Hydrogen Energy Laboratory, Ural Federal University, 620002 Yekaterinburg, Russia*

[c] *State Key Laboratory for Mechanical Behaviour of Materials, School of Materials Science and Engineering, Xi'an Jiaotong University, Xi'an Shannxi 710049, China*

[d] *Department of Inorganic Chemistry, Faculty of Natural Sciences, Comenius University in Bratislava, 842 15 Bratislava, Slovakia*

† Electronic supplementary information (ESI) available: Table S1, the ionic conductivity of solid oxide thin-film electrolytes under SOFC/SOEC operation. See DOI: **https://doi.org/10.1039/d4ta03852e**

strategy involves reducing the electrolyte thickness (*i.e.*, thin film technologies[29–33]), which naturally decreases the ohmic resistance of the cells. The second strategy entails the replacement of zirconia materials with more conductive analogs that exhibit the requisite conductivity values at reduced operation temperatures.[34–36] The simultaneous use of these two strategies allows a significant reduction in operating temperatures down to a range of 400–600 °C, which is sufficient to achieve the desired performance of SOFCs and SOECs.

There are numerous types of highly conductive ionic electrolytes with varying structures or ionic transport characteristics. However, fluorite-based and perovskite-based complex oxides remain the most extensively studied systems for SOFC and SOEC applications. This perspective presents a comparative analysis of the ionic conductivity of electrolytes. First, it examines trends identified many years ago (Section 2). We then conducted a meticulous analysis of possible approaches for achieving the highest conductivities for each discussed class (Sections 3.1–3.7). The SOFC and SOEC electrolytes must possess pure ionic transport with very low (negligible) electronic conduction to offer high-efficient electrochemical conversion. However, unipolar transport is difficult to achieve for the considered systems. Therefore, Section 3.8 provides some insight into this matter. Finally, the ionic conductivity of the electrolytes as part of solid oxide electrochemical cells was also analyzed (Section 4). All of the above allowed us to conduct a revision in the field of ionic conductivity and clarify the positions of different electrolytes relative to each other.

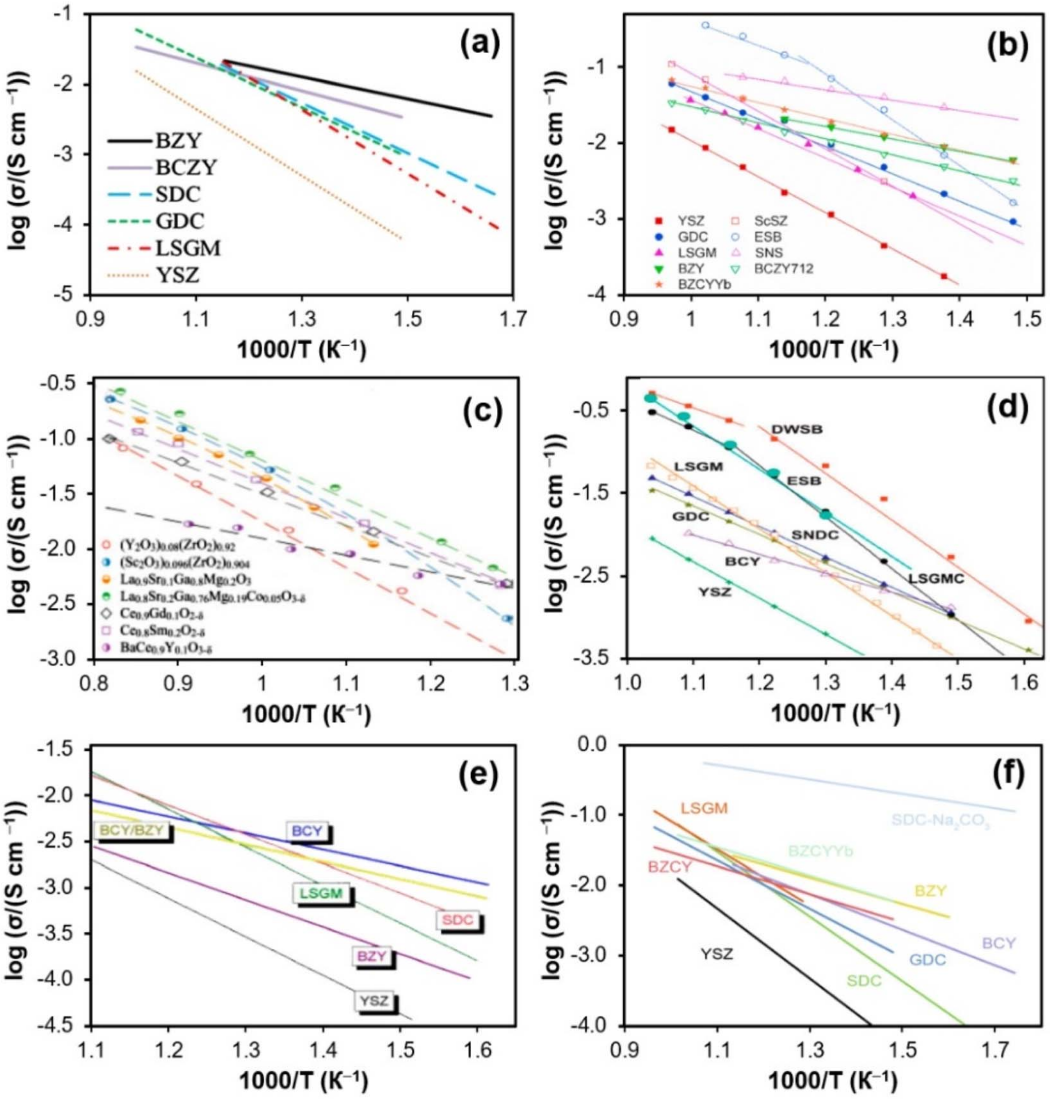

Fig. 1 Electrical conductivity of the SOFC and SOEC electrolyte materials: Y-doped or Sc-doped $ZrO_2$ (YSZ, ScSZ), Sm-doped or Gd-doped $CeO_2$ (SDC, GDC) fluorite oxides; $LaGaO_3$-based (LSGM) and widely studied Ba-based cerates (BCY), zirconates (BZY), and their solid solutions (BCZY, BZCYYb) perovskites. These data were obtained from the works of (a) Volkov *et al.*, reproduced with permission from ref. 51. Copyright 2017, Elsevier B.V.; (b) Shi *et al.*, reproduced with permission from ref. 52. Copyright 2020, Elsevier B.V.; (c) Gómez *et al.*, reproduced with permission from ref. 53. Copyright 2016, Elsevier Ltd.; (d) Vostakola *et al.*, reproduced with permission from ref. 54 as an open access source; (e) Fabbri *et al.*, reproduced with permission from ref. 55. Copyright 2010, Taylor & Francis Informa UK Ltd – Journals; and (f) Su *et al.* reproduced with permission from ref. 56. Copyright 2020, Elsevier B.V.

## 2 A brief introduction to solid oxide electrolytes

The electrolyte is a crucial functional material in SOFCs/SOECs, facilitating the conduction of ions through its dense body and the separation of cathode and anode spaces, preventing the mixing of oxidizing and reducing gas atmospheres. The electrolyte must fulfill a number of rigorous requirements, including high ionic conductivity, low electronic conductivity, excellent gas-tightness, and chemical stability against gas environments and other functional materials. It is evident that a complete alignment with these requirements represents a significant challenge. Consequently, numerous research initiatives have been undertaken with the objective of identifying suitable oxide matrixes as alternatives to conventional zirconia electrolytes. While many exotic electrolyte systems have been recently proposed, fluorite- and perovskite-based oxides remain the state-of-the-art materials for the design of promising electrolytes. These oxides include doped $CeO_2$ (ref. 37–40) and doped $LaGaO_3$,[41,42] which act as oxygen-ionic conductors, and doped $Ba(Ce,Zr)O_3$ (ref. 43–46) and doped $BaZrO_3$,[47–50] which act as protonic conductors.

It is widely recognized that the ionic conductivity of the mentioned electrolytes exceeds that of YSZ by several times to several orders of magnitude, as evidenced by comparative graphs extracted from the literature sources (see Fig. 1).[51–56] However, the ionic conductivity of alternative electrolytes often differs in terms of the absolute values for certain materials and their positions relative to each other. There are several reasons for the inconsistency of these results:

(1) The ionic conductivity data are typically derived from different studies. However, in each case, the transport properties are significantly influenced by the actual chemical composition and microstructural parameters of the ceramics, which depend on the technological regimes of powder preparation and ceramic fabrication. Consequently, the ionic conductivity can exhibit a considerable degree of variability even for the same nominal compositions.

(2) The comparison is typically provided for oxidizing conditions (Fig. 1). However, Ba-based perovskites exhibit p-type electronic conductivity under oxidizing environments.[57] Moreover, their ionic conductivity increases as the water vapor partial pressure increases due to a change in the nature of the conductivity from oxygen-ionic to co-ionic or protonic. In principle, the comparison of the ionic conductivity for all electrolytes can be provided for wet reducing atmospheres, where Ba-based perovskites are purely ionic conductors. However, another electrolyte class, doped $CeO_2$ materials, exhibits n-type electronic conductivity at low oxygen partial pressures,[39,40] thus limiting the applicability of this comparison between different electrolyte classes.

(3) Discussing the features of proton-conducting materials,[43–50] their oxygen-ionic and protonic conductivities are regulated not only by water vapor partial pressure but also by temperature. In detail, the heating process results in water desorption from the structure of the protonic conductors, decreasing the proton concentration and proton conductivity (see Section 3.8 below). This process is especially intensive at temperatures above 600 °C. When the proton conductivity decreases, a simultaneous increase in the oxygen-ionic conductivity occurs due to the generation of additional oxygen vacancies.

The data presented in Fig. 1 pertain to the materials studied in certain studies. Therefore, it is challenging to draw a definitive conclusion regarding which materials exhibit the highest ionic conductivity. To elucidate this aspect in greater detail, the subsequent section will provide a concise overview of the electrical properties for each specific electrolyte system. In addition to their transport features, the main advantages and limitations will also be presented.

## 3 Ionic conductivity of solid oxide ceramic electrolytes

This section presents a discussion of the nature of ionic conductivity in oxygen-ionic and proton-conducting electrolytes, as well as an examination of the detrimental factors that can deteriorate their transport properties. Additionally, this section includes experimental conductivity data for each electrolyte class. Since abundant data can be found in the literature, we limited the presented graphs to at least 10 literature sources indicating possible variations in conductivity. It should be noted that dependencies that deviated significantly from the general trends (in absolute conductivity values or slopes) for any considered system were excluded from the comparative analysis.

### 3.1. Conventional YSZ materials

YSZ is one of the most extensively studied materials for SOFC and SOEC applications, encompassing both laboratory and commercial applications. Yttria ($Y_2O_3$) is introduced to zirconia to stabilize the crystal structure of $ZrO_2$; at room temperature, $ZrO_2$ exhibits a monoclinic structure, which first transforms to a tetragonal phase and then to a cubic phase at ~1170 and 2370 °C, respectively.[37,58] For YSZ, Y-introduction plays several important roles. First, it stabilizes the distorted structures to the cubic phase, which offers high ionic conductivity under operating conditions due to a high cubic symmetry. Second, yttrium acts as an acceptor dopant, resulting in the formation of oxygen vacancies that regulate the oxygen-ionic conductivity. An 8YSZ composition (*i.e.*, $(ZrO_2)_{0.92}(Y_2O_3)_{0.08}$) is considered to be the best over a range of single-phase materials. At other yttrium concentrations, the ionic conductivity decreases due to a lower concentration of oxygen vacancies as main charge carriers or defect interactions (associations) occurring in the heavily doped $ZrO_2$.

The ionic conductivity of YSZ is dependent on a number of factors, including the type and concentration of dopant. However, the ionic conductivity of the same 8YSZ composition can vary significantly (Fig. 2), indicating that the technological parameters play a pivotal role in the preparation of ceramic bodies. The grain size, type/concentration of uncontrolled

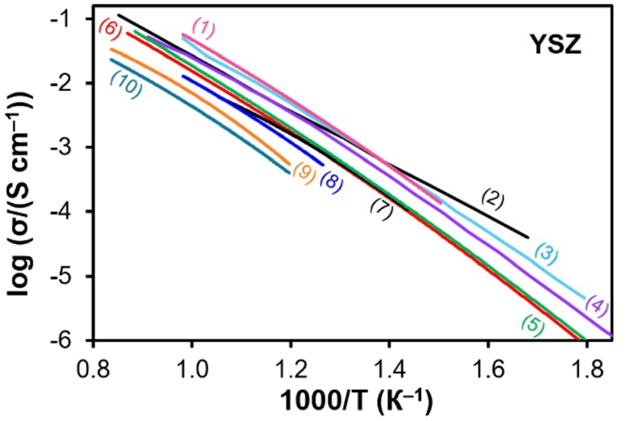

Fig. 2 Temperature dependencies of electrical conductivity for YSZ materials extracted from different sources: (1) – ref. 59; (2) – ref. 60; (3) – ref. 61; (4) – ref. 62; (5) – ref. 62; (6) – ref. 63; (8) – ref. 64; (7) – ref. 65; (9) – ref. 66; (10) – ref. 66.

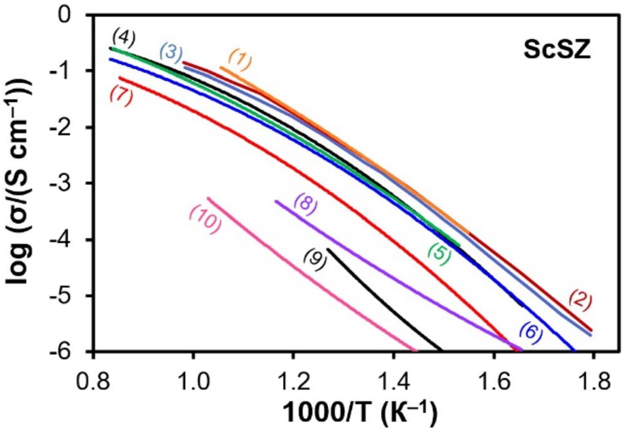

Fig. 3 Temperature dependencies of electrical conductivity for ScSZ materials extracted from different sources: (1) – ref. 65; (2) – ref. 68; (3) – ref. 61; (4) – ref. 69; (5) – ref. 70; (6) – ref. 71; (7–10) – ref. 69.

impurities, and relative density are the primary factors influencing the observed conductivity variation. The optimal 8YSZ ceramic is capable of reaching 50 mS cm$^{-1}$ at 800 °C and 150 mS cm$^{-1}$ at 1000 °C, although several highly conductive 8YSZ materials can be found in the literature. Nevertheless, these ionic conductivities remain relatively low, prompting the search for new electrolytes of the same or other oxide matrixes.

### 3.2. Zirconia materials: beyond YSZ

Scandia-stabilized zirconia (ScSZ or SSZ) represents an alternative family of zirconia electrolytes, whose ionic conductivity exceeds that of YSZ by 3–10 times depending on temperature. The higher ionic conductivity of the Sc-containing electrolytes is attributed to the close ionic radii of $Sc^{3+}$ and $Zr^{4+}$ (0.87 and 0.84 Å, respectively). Such an ionic radii compatibility offers a low elastic strain and a low activation energy for the diffusion of oxygen vacancies, both of which facilitate better ionic conductivity compared to the Y-containing counterparts.[67] If the maximum conductivity corresponds to ∼8 mol% for the YSZ system, the ScSZ system exhibits a conductivity maximum at 10–11 mol%. At higher scandium concentrations, a rhombohedral $ZrO_2$-based phase starts to appear, while a tetragonal phase remains stable at lower Sc-contents (below 7 mol%). Consequently, the concentration maximum of the ionic conductivity is associated with the formation of a highly symmetric (cubic) structure coupled with a relatively high concentration of oxygen vacancies.

As illustrated in Fig. 3, the absolute ionic conductivity values for ScSZ are generally greater than those of YSZ, demonstrating, at the same time, a considerable range of conductivity variation. As stated above, this phenomenon can be attributed to the distinct microstructural properties of the prepared ceramics. Despite exhibiting superior transport properties, Sc-containing zirconia has been found to be deficient in chemical stability in the long-term prospect.[58,72] Numerous studies have shown that the ionic conductivity of ScSZ ceramics significantly decreases (degrades) as a consequence of the high-temperature phase transformation (from cubic to tetragonal or rhombohedral structures) and the segregation of secondary phases at grain boundaries of the ceramics. In contrast, YSZ materials exhibit better chemical stability.

The undesirable processes that occur in ScSZ can be purposefully eliminated by changing the Sc-content and introducing additional dopants. In detail, co-doping strategy allows a compromise between stability and conductivity to be achieved. The most frequently used co-dopants for ScSZ are cerium, yttrium, and ytterbium,[67] although some studies have reported successful results on the co-doping of ScSZ with aluminum, niobium, manganese, bismuth, or titanium.[72]

### 3.3. $CeO_2$-based materials

$CeO_2$ is a promising oxide matrix for the design of highly conductive oxygen-ionic electrolytes.[37,73] Ceria and its doped derivatives ($Ce_{1-x}M_xO_{2-\delta}$, $x \le 0.3$; where M is the alkaline earth or rare earth element) exhibit a fluorite-like structure similar to that of their $ZrO_2$-based counterparts. In addition to higher ionic conductivity, $CeO_2$-based materials are characterized by better chemical compatibility with various functional materials. As a result, doped $CeO_2$ is often used as a protective layer for SOFCs and SOECs with YSZ or ScSZ thin-film electrolytes.[74,75]

The oxygen-ionic conductivity of doped ceria reaches its maximum at 15–20 mol% of an acceptor dopant, with samarium and gadolinium being considered the best dopants.[38,40,76,77] It is interesting to note that $Ce_{0.8}Sm_{0.2}O_{2-\delta}$ (SDC or CSO) is the most extensively studied member of the $Ce_{1-x}Sm_xO_{2-\delta}$ series, while a $Ce_{0.9}Gd_{0.1}O_{2-\delta}$ (GDC or CGO) composition with a lower dopant concentration is the most studied member of the $Ce_{1-x}Gd_xO_{2-\delta}$ series. In principle, theoretical calculations of $CeO_2$ transport properties have demonstrated that the maximum ionic conductivity should be observed near 10 mol%, taking the blocking and trapping effects of oxygen vacancies with lanthanide dopants into account.

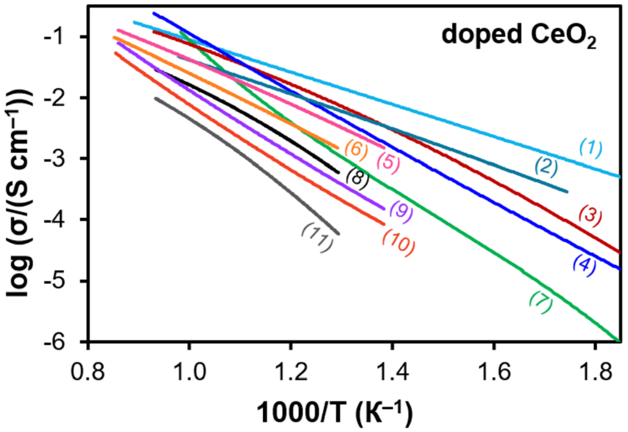

**Fig. 4** Temperature dependencies of electrical conductivity for doped $CeO_2$ materials extracted from different sources: (1) $Ce_{0.9}Gd_{0.1}O_{2-\delta}$;[60] (2) $Ce_{0.8}Gd_{0.2}O_{2-\delta}$;[80] (3) $Ce_{0.9}Nd_{0.1}O_{2-\delta}$;[81] (4) $Ce_{0.8}Nd_{0.2}O_{2-\delta}$;[81] (5) $Ce_{0.8}Sm_{0.2}O_{2-\delta}$;[82] (6) $Ce_{0.85}Sm_{0.15}O_{2-\delta}$;[82] (7) $Ce_{0.9}Gd_{0.1}O_{2-\delta}$;[81] (8) $Ce_{0.75}Sm_{0.25}O_{2-\delta}$;[83] (9) $Ce_{0.8}Gd_{0.2}O_{2-\delta}$;[82] (10) $Ce_{0.85}Gd_{0.15}O_{2-\delta}$;[82] (11) $Ce_{0.95}Sm_{0.05}O_{2-\delta}$.[83]

One of the major drawbacks of ceria electrolytes is their tendency to undergo partial $Ce^{4+}$-to-$Ce^{3+}$ transformation in highly reducing environments,[39,40] including hydrogen, methane, $CO_2$ + CO, and other gas mixtures. Such a cationic reduction is accompanied by the appearance of n-type electron conductivity, which is detrimental to SOFCs, and especially SOECs. In detail, the high electronic conductivity in the electrolyte causes an internal short circuit, which considerably reduces the energy conversion efficiency. There are many technological strategies to inhibit the electronic conductivity under fuel cell and electrolysis cell operations, but they often represent a trade-off between different functional properties. Another consequence of cationic reduction is chemical expansion as a mechanical response to dimensional variations in cationic and anionic sizes.[78,79] This can also have a detrimental effect on the SOFC/SOEC performance due to the appearance of mechanical stresses between different functional layers.

Fig. 4 shows the ionic conductivity of the doped ceria materials across a broad temperature range. As observed in the previous graphs, the conductivity can exhibit a considerable range of variation even for the same electrolyte composition at the same temperature. This further substantiates the assertion that not only chemical and structural factors but also microstructural parameters influence the transport properties of the corresponding ceramics. When the absolute ionic conductivity values are compared, it is evident that $CeO_2$-based materials exhibit superior performance compared to their zirconia-based counterparts: their high ionic conductivity can be achieved at temperatures by 100–200 °C lower than that of zirconia electrolytes.

### 3.4. $LaGaO_3$-based materials

$LaGaO_3$ is a member of the La-containing perovskite family, which is defined by the $La^{3+}M^{3+}O_3$ stoichiometry, where M can consist of p-, d-, or f-elements. Examples of La-based perovskites include $LaGaO_3$, $LaScO_3$, and $LaYbO_3$. The ionic radius of the B-site basic elements[84] determines whether the corresponding phases exhibit pure oxygen-ionic conductivity (*e.g.*, aluminates and gallates) or protonic conductivity (*e.g.*, indates, scandates, yttrates, and ytterbates). The hydration capability of such oxides is regulated by their crystal features (size and symmetry of the perovskite structure) as well as features related to the coordination preference of the B-site cations. In detail, the structures of the original and doped $LaAlO_3$ and $LaGaO_3$ are characterized by small sizes, while aluminum and gallium are stable in four coordination environments.[85] This explains why these phases are predominantly oxygen-conducting electrolytes and have no notable capability towards hydration.

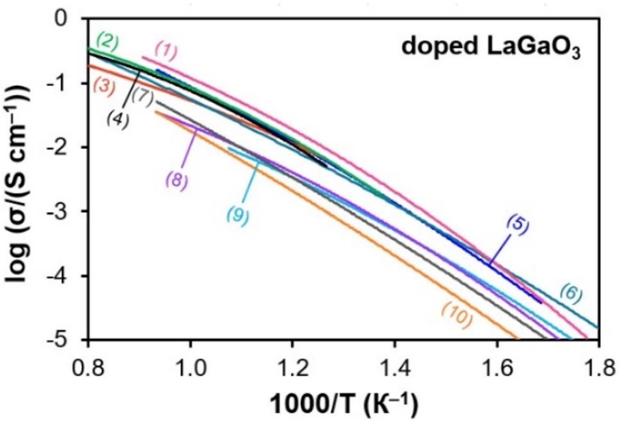

**Fig. 5** Temperature dependencies of electrical conductivity for doped $LaGaO_3$ materials extracted from different sources: (1) $La_{0.8}Sr_{0.2}Ga_{0.8}Mg_{0.2}O_{3-\delta}$;[87] (2) $La_{0.9}Sr_{0.1}Ga_{0.8}Mg_{0.2}O_{3-\delta}$;[88] (3) $La_{0.9}Sr_{0.1}Ga_{0.9}Mg_{0.1}O_{3-\delta}$;[89] (4) $La_{0.8}Sr_{0.2}Ga_{0.8}Mg_{0.2}O_{3-\delta}$;[90] (5) $La_{0.85}Sr_{0.15}Ga_{0.8}Mg_{0.2}O_{3-\delta}$;[91] (6) $La_{0.9}Sr_{0.1}Ga_{0.8}Mg_{0.2}O_{3-\delta}$;[92] (7) $La_{0.9}Sr_{0.1}Ga_{0.9}Mg_{0.1}O_{3-\delta}$;[93] (8) $La_{0.9}Sr_{0.1}Ga_{0.8}Mg_{0.2}O_{3-\delta}$;[94] (9) $La_{0.8}Sr_{0.2}Ga_{0.85}Mg_{0.15}O_{3-\delta}$;[95] (10) $La_{0.8}Sr_{0.2}Ga_{0.8}Mg_{0.2}O_{3-\delta}$.[96]

Compared to $LaAlO_3$ and $LaGaO_3$ materials, aluminates are characterized by a very low oxygen-ion conductivity of approximately 5 mS cm$^{-1}$ at 800 °C.[41] In other words, the ionic conductivity of aluminates is even lower than that of zirconia. This is due to the very dense packing structure of $LaAlO_3$, which provides narrow channels for oxygen diffusion. $LaGaO_3$ has a larger free volume, which facilitates oxygen transport; in addition, the optimized structural features of gallates allow them to achieve one of the highest ionic conductivity values, up to 150 mS cm$^{-1}$ at 800 °C. Due to their superior conductivity, $LaGaO_3$-based SOFCs are capable of demonstrating satisfactory performance in an electrolyte-support configuration, in contrast to other SOFCs, which are typically based on thin-film electrolyte design.

The most conductive gallates are formed from a $La_{1-x}Sr_xGa_{1-y}Mg_yO_{3-\delta}$ series (LSGM[42,86]), where both the La- and Ga-sites are partially substituted with the $Sr^{2+}$ and $Mg^{2+}$ acceptor dopants, respectively. Numerous investigations have shown that the most optimal Mg content corresponds to $y = 0.2$, while the La-with-Sr substitution can vary from $x = 0.1$ to $x = 0.2$. Such a combination of dopant types and their content

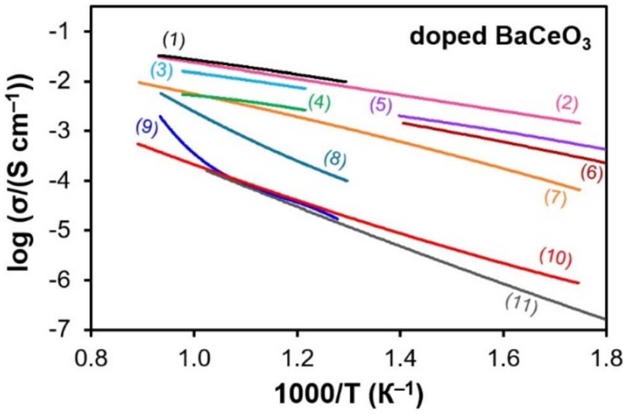

Fig. 6 Temperature dependencies of electrical conductivity for doped $BaCeO_3$ materials extracted from different sources: (1) $BaCe_{0.8}Y_{0.2}O_{3-\delta}$;[99] (2) $BaCe_{0.85}Er_{0.15}O_{3-\delta}$;[100] (3) $BaCe_{0.9}Y_{0.1}O_{3-\delta}$;[101] (4) $BaCe_{0.85}Y_{0.1}In_{0.05}O_{3-\delta}$;[101] (5) $BaCe_{0.9}Y_{0.1}O_{3-\delta}$;[102] (6) $BaCe_{0.9}Gd_{0.1}O_{3-\delta}$;[102] (7) $BaCe_{0.9}Y_{0.1}O_{3-\delta}$;[103] (8) $BaCe_{0.75}Y_{0.25}O_{3-\delta}$;[104] (9) $BaCe_{0.9}Y_{0.1}O_{3-\delta}$;[104] (10) $BaCe_{0.9}Sm_{0.1}O_{3-\delta}$;[103] (11) $BaCe_{0.9}Y_{0.1}O_{3-\delta}$.[105]

generates oxygen vacancies and minimally affects the lattice distortion at the same time. Both of these factors contribute to the high ionic conductivity of gallates (Fig. 5). The use of dopants other than $Sr^{2+}$ and $Mg^{2+}$ is often associated with a considerable reduction in ionic conductivity.

Despite the very high ionic conductivity of gallates, these materials suffer from chemical stability issues during materials processing or their long-term operation. These problems are attributed to the relatively rapid diffusion of $La^{3+}$ (compared to other cations) as well as the potential volatility of gallium at very high sintering temperatures required for the desirable sinterability of the corresponding ceramics. As a result, new impurity phases based on $LaSrGaO_4$ and $SrLaGa_3O_7$ are formed along the grain boundaries during high temperature treatments. These phases are poorly conductive, with ionic conductivity lower by 4–5 orders of magnitude than that of the LSGM phases.[74]

### 3.5. $BaCeO_3$-based materials

Barium cerate ($BaCeO_3$) is a well-known representative of perovskite phases with pronounced proton transport at elevated temperatures.[97,98] Doped $BaCeO_3$ materials exhibit the highest proton conductivity reported to date due to the large crystal structure and strong basic character of both the A- and B-site cations. The typical temperature dependences of the ionic conductivity are shown in Fig. 6.

The most promising dopants for the $BaCeO_3$ matrix are yttrium, gadolinium, and samarium. They typically form highly conductive materials at 10–20 mol% of dopants.[106] However, at higher dopant concentrations, the conductivity of the cerates decreases for several possible reasons, including defect association or passing through a solid solution boundary, when impurity phase(s) might form. In addition to conventional doping, co-doping with different lanthanides represents a promising approach for enhancing proton conductivity in cerates.[107–111]

Another considerable drawback of cerates is their low chemical stability against $CO_2$ and even steam.[112] Due to its pronounced basic character, $BaCeO_3$ easily interacts with gas components and decomposes, thereby losing its proton-conducting behavior. Although the chemical stability of cerates can be partially improved *via* their co-doping by stabilizing elements (for example, $Ga^{3+}$, $In^{3+}$, $Zr^{4+}$, $Sn^{4+}$, $Nb^{5+}$ and $Ta^{5+}$),[106] many researchers are looking for other oxide matrixes with enhanced proton transport.

It should be noted that $BaCeO_3$, as well as other Ba-containing perovskites, are not pure protonic conductors since meaningful oxygen-ionic and p-type electronic transport can be realized depending on external parameters.[57,113] In detail, the oxygen-ionic conductivity prevails over the protonic conductivity in dry atmospheres. Conversely, the hole conductivity is more pronounced than the ionic conductivity under oxidizing conditions at elevated temperatures (above 700 °C). In other words, Ba-containing perovskites exhibit triple-conducting behavior, which is extremely promising for electrode systems.[114–116] However, this is not a desirable property for electrolytes. Due to the mixed type of transport, a more accurate comparison of the ionic conductivity for protonic materials can be made for wet reducing atmospheres, where the p-type electronic conductivity is significantly diminished. However, even within the electrolyte domain boundary, the ionic conductivity in wet reducing atmospheres undergoes a transition from protonic to oxygen-ionic as the temperature increases due to dehydration of the material.

### 3.6. $BaZrO_3$-based materials

Barium zirconate ($BaZrO_3$) is another representative of proton-conducting perovskites that demonstrates very high chemical stability in different environments (including $CO_2$ and $H_2S$-containing atmospheres) and no phase transitions from room to operating temperatures.[47–49,117] It is widely accepted that doped $BaZrO_3$ displays the highest (bulk) protonic conductivity among other perovskites (Fig. 1a and f). Nevertheless, other studies have indicated that Ce-enriched compounds (including doped cerates) exhibit greater conductivity than that of pure zirconates (Fig. 1b and e).

In the context of the doped $BaZr_{1-x}M_xO_{3-\delta}$ series, $Y^{3+}$ and $Sc^{3+}$ are considered to be the most suitable dopants for achieving high proton conductivity.[49,117] Nevertheless, Y-doped derivatives have been widely explored for experimental and applied purposes due to the broader availability and lower cost of yttrium chemicals. Among the $BaZr_{1-x}Y_xO_{3-\delta}$ derivatives, the highest protonic conductivity is achieved for $x \approx 0.2$,[118,119] as shown in Fig. 7.

Like doped $BaCeO_3$, barium zirconates are triple-conductor materials with predominantly p-type electronic conductivity under oxidizing conditions and elevated temperatures. Comparative analysis of the electronic transport of cerates and zirconates conducted by independent researchers[130–132] has demonstrated that doped $BaZrO_3$ exhibits greater electronic conductivity than doped $BaCeO_3$ under comparable conditions. Consequently, the use of pure zirconates as thin-film

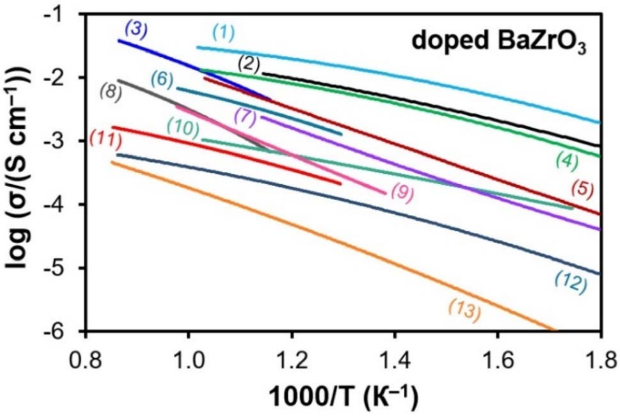

Fig. 7 Temperature dependencies of electrical conductivity for doped $BaZrO_3$ materials extracted from different sources: (1) $BaZr_{0.77}Y_{0.23}O_{3-\delta}$;[119] (2) $BaZr_{0.8}Y_{0.2}O_{3-\delta}$;[120] (3) $BaZr_{0.8}Y_{0.2}O_{3-\delta}$;[121] (4) $Ba_{0.98}Zr_{0.8}Y_{0.2}O_{3-\delta}$;[119] (5) $BaZr_{0.85}Y_{0.15}O_{3-\delta}$;[122] (6) $BaZr_{0.8}Y_{0.2}O_{3-\delta}$;[123] (7) $BaZr_{0.8}Y_{0.2}O_{3-\delta}$;[124] (8) $BaZr_{0.95}Y_{0.05}O_{3-\delta}$;[121] (9) $BaZr_{0.85}Y_{0.15}O_{3-\delta}$;[125] (10) $BaZr_{0.8}Y_{0.2}O_{3-\delta}$;[126] (11) $BaZr_{0.9}Y_{0.1}O_{3-\delta}$;[127] (12) $BaZr_{0.8}Y_{0.2}O_{3-\delta}$;[128] (13) $BaZr_{0.7}Y_{0.3}O_{3-\delta}$.[129]

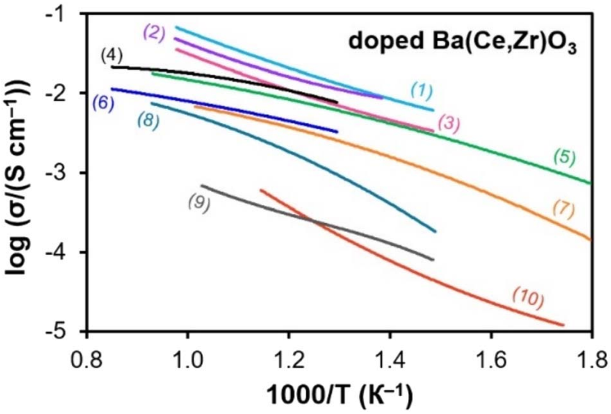

Fig. 8 Temperature dependencies of electrical conductivity for doped $Ba(Ce,Zr)O_3$ materials extracted from different sources: (1) $BaCe_{0.7}Zr_{0.1}Y_{0.1}Yb_{0.1}O_{3-\delta}$;[138] (2) $BaCe_{0.7}Zr_{0.1}Y_{0.1}Yb_{0.1}O_{3-\delta}$;[139] (3) $BaCe_{0.7}Zr_{0.1}Y_{0.2}O_{3-\delta}$;[138] (4) $BaCe_{0.5}Zr_{0.3}Y_{0.2}O_{3-\delta}$;[140] (5) $BaCe_{0.7}Zr_{0.1}Y_{0.1}Yb_{0.1}O_{3-\delta}$;[141] (6) $BaCe_{0.5}Zr_{0.3}Y_{0.05}Yb_{0.15}O_{3-\delta}$;[140] (7) $BaCe_{0.3}Zr_{0.55}Y_{0.15}O_{3-\delta}$;[142] (8) $BaCe_{0.7}Zr_{0.1}Y_{0.1}Yb_{0.1}O_{3-\delta}$;[143] (9) $BaCe_{0.7}Zr_{0.1}Y_{0.2}O_{3-\delta}$;[144] (10) $BaCe_{0.5}Zr_{0.4}Y_{0.1}O_{3-\delta}$.[145]

electrolytes for protonic ceramic electrolysis cells is challenging (due to their high electronic leakage); however, these materials can be utilized for protonic ceramic fuel cells, whose overall energy conversion efficiency is found to be adequate despite the presence of hole conductivity.[131]

Another well-known problem of zirconates is their extremely high grain boundary resistivity due to poor densification and grain growth. This reduces the overall proton conductivity of zirconates, making them less conductive than the Ce-containing perovskites. This problem can be addressed by wet chemical solution methods or by adding small amounts of sintering additives.[47,133] However, both approaches have their own limitations that require careful optimization of the synthesis/sintering regimes in each specific case related to the preparation of gas-tight $BaZrO_3$-based ceramics.

### 3.7. $Ba(Ce,Zr)O_3$-based materials

Cerate zirconates ($Ba(Ce,Zr)O_3$) represent a common system composed of both $BaCeO_3$ and $BaZrO_3$ phases in the form of solid solutions, *i.e.*, $BaCe_{1-x-y}Zr_xM_yO_{3-\delta}$. In such solid solutions, the Ce-to-Zr ratio can vary widely (from pure cerates to pure zirconates), providing the advantages of basic oxides:[44,134] high ionic conductivity, acceptable sinterability, and good chemical stability.

Among cerate-zirconates, Y-doped materials are the most extensively studied examples. Over an extended period, researchers have concentrated their attention on a $BaCe_{0.7}Zr_{0.1}Y_{0.2}O_{3-\delta}$ compound (also designated $BaZr_{0.1}Ce_{0.7}Y_{0.2}O_{3-\delta}$) due to its exceptionally high protonic conductivity.[135–137] Indeed, this complex oxide is situated adjacent to the cerate family, with a slight Ce-with-Zr substitution in $BaCeO_3$. Consequently, both the bulk and total conductivities of $BaCe_{0.7}Zr_{0.1}Y_{0.2}O_{3-\delta}$ were found to be highly promising (Fig. 8). Further studies have demonstrated that 10 mol% $Zr^{4+}$ is insufficient to maintain the desired chemical stability of $Ba(Ce,Zr)O_3$ in $CO_2$-containing atmospheres. Consequently, the zirconium concentration is often increased to 30–50 mol%, although this may entail a trade-off in transport properties.[146–149]

To enhance the ionic conductivity at a specific Ce-to-Zr ratio, co-doping represents a prevalent chemical design strategy. Numerous independent studies have demonstrated that Y- and Yb-co-doped cerate zirconates exhibit enhanced conductivity relative to their single-doped counterparts.[43] Other lanthanides can also be introduced into cerate zirconates until the formation of high-entropy oxides.[150–153]

### 3.8. Transport features for oxygen-ionic and proton-conducting electrolytes: similarity and contrast

The previous subsections dealt with a brief discussion of electrolyte materials capable of oxygen-ionic or proton transport. Considering each electrolyte family, it was pointed out that some of them exhibit the 'foreign' conductivity(ies) due to its own chemical or structural features. The present subsection provides the basic information in this regard, highlighting the reasons for the appearance of other conductivity types and possible ways to separate the partial conductivities from each other.

Stabilized zirconia electrolytes are distinguished by unipolar oxygen-ionic transport across the experimentally achieved SOFC/SOEC operation, including both oxidizing and reducing atmospheres. The oxygen-ionic conductivity of the stabilized $ZrO_2$ complex oxides is primarily influenced by oxygen vacancies introduced by impurity doping. In the case of YSZ, such an impurity disordering process can be presented through a quasi-chemical formalism as follows:

$$Y_2O_3 \xrightarrow{ZrO_2} 2Y'_{Zr} + V_O^{\bullet\bullet} + 3O_O^{\times} \qquad (1)$$

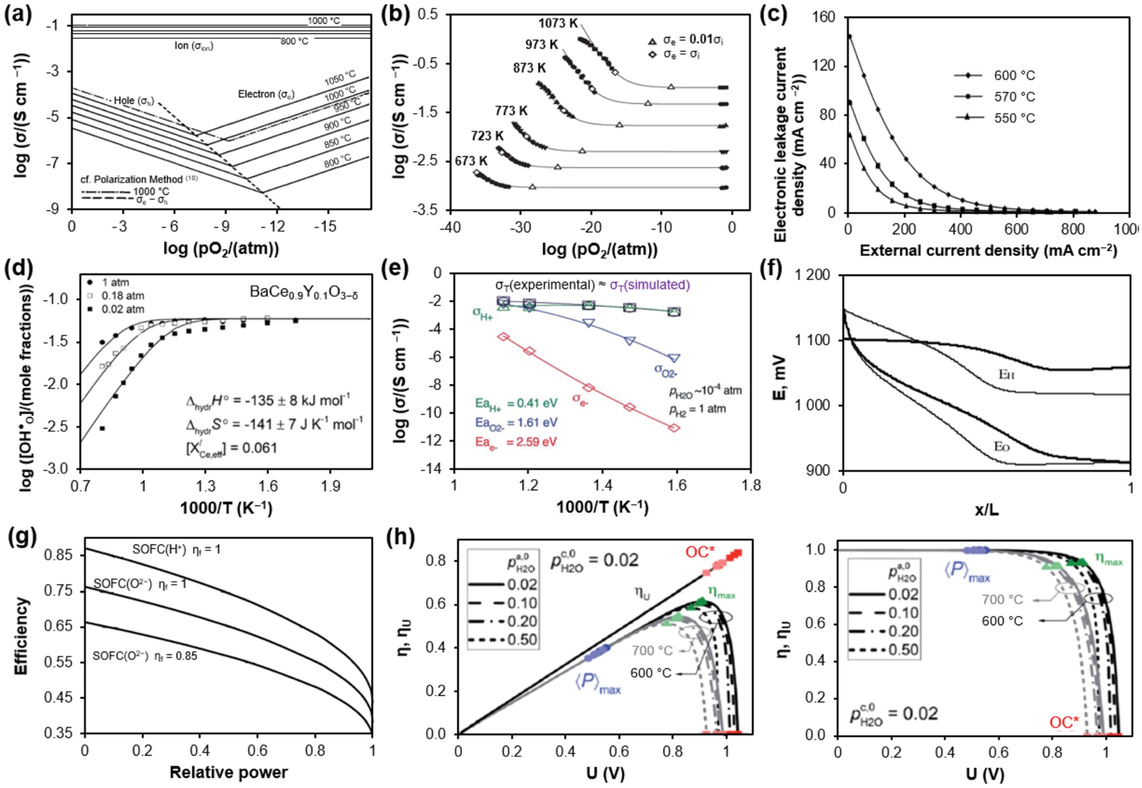

Fig. 9 Selected results regarding individual transport properties of oxygen-ionic and proton-conducting electrolytes: (a) partial conductivities of YSZ depending on $pO_2$ at different temperatures. Reproduced with permission from ref. 154. Copyright 1989, ECS – The Electrochemical Society; (b) total conductivity of $Ce_{0.8}Sm_{0.2}O_{2-\delta}$ as a function of $pO_2$ at different temperatures. Reproduced with permission from ref. 157. Copyright 2004, Elsevier B.V.; (c) electronic leakage current density through the doped $CeO_2$ electrolyte as a function of external circuit current density at different temperatures with a fuel mixture of 3% $H_2O/H_2$. Reproduced with permission from ref. 158. Copyright 2005, Elsevier B.V.; (d) temperature dependences of proton concentration in $BaCe_{0.9}Y_{0.1}O_{3-\delta}$. Reproduced with permission from ref. 159. Copyright 2015, The Royal Society of Chemistry; (e) temperature dependences of the total and partial conductivities of $BaCe_{0.9}Y_{0.1}O_{3-\delta}$ in wet hydrogen. Reproduced with permission from ref. 160. Copyright 2019, The Royal Society of Chemistry; (f) distributions of the cell potential for PCFCs and SOFCs in co-flow and count-flow modes. Reproduced with permission from ref. 164. Copyright 2004, Elsevier B.V.; (g) efficiency of PCFC and SOFC depending on their relative power. Reproduced with permission from ref. 165. Copyright 2001, International Association for Hydrogen Energy; (h) overall, voltage, and faradaic efficiencies as a function of the cell voltage at different values of the inlet fuel humidity and temperature. Reproduced with permission from ref. 166. Copyright 2020, The Royal Society of Chemistry.

As can be see, an impurity element must possess a lower oxidation state than that of a replaceable cation; as a result, double positively charged oxygen vacancies emerge in a crystal structure to compensate for the negatively charged defects (yttrium cations in the zirconium regular positions of the crystal, as exemplified by the aforementioned case).

Principally, electron defects can also appear owing to the interaction of point defects with a gas phase. In the case of oxidizing atmospheres, holes might be formed upon the oxygen adsorption process:

$$V_O^{\bullet\bullet} + 1/2O_2 \rightleftarrows O_O^{\times} + 2h^{\bullet} \tag{2}$$

On the contrary, if the oxygen chemical activity in a reducing atmosphere is much lower than that in a solid oxide, oxygen desorption is possible, which results in the formation of electrons:

$$O_O^{\times} \rightleftarrows V_O^{\bullet} + 1/2O_2 + 2e' \tag{3}$$

Applying the low of mass action, the p-type and n-type electronic conductivities are proportional to oxygen partial pressure ($pO_2$) as $\sigma_p \sim [h^{\bullet}] \sim (pO_2)^{1/4}$ and $\sigma_n \sim [e'] \sim (pO_2)^{-1/4}$, respectively.

SOFCs and SOECs based on stabilized zirconia materials typically demonstrate open circuit voltage (OCV) values that are in close alignment with the theoretical values (calculated by the Nernst equation) in the case of gas-tight (dense) electrolyte layers. This means that no meaningful electronic transport exists in such a kind of materials, if they do not contain transition-type elements. Indeed, under real experimental conditions, the n- or p-type electronic conductivity is found to be 3–4 orders of magnitude lower than oxygen-ionic conductivity,[154–156] see Fig. 9a. In other words, the oxygen-ionic transference number of $ZrO_2$-based electrolytes is nearly equal to 1, resulting in no decline in OCVs. According to the data presented in Fig. 9a, the n-type electronic conductivity becomes equal to the ionic one at the $pO_2$ values of $10^{-40}$ atm at 800 °C and $10^{-29}$ atm at 1000 °C. These values are considerably lower than those observed in experiments. For example, a gas mixture of 1% $H_2O$ in $H_2$ is characterized by the $pO_2$ values of $4.6 \times 10^{-23}$ and $2.9 \times 10^{-19}$ atm at 800 and 1000 °C, respectively. The same unipolar oxygen-ionic transport is observed for doped $LaGaO_3$ electrolytes in the case of stable oxidation states for both basic and doped cations.

As previously mentioned in Section 3.3, $CeO_2$-based materials display not only oxygen-ionic conductivity, but also n-type electronic conductivity in reducing atmospheres. The source of electrons is attributed to the transition behavior of Ce-ions, whereby a partial $Ce^{4+}$ to $Ce^{3+}$ reduction occurs under low $pO_2$ values:[39,40]

$$2\mathrm{Ce}_{\mathrm{Ce}}^{\times} + \mathrm{O}_{\mathrm{O}}^{\times} \rightleftarrows 2\mathrm{Ce}_{\mathrm{Ce}}^{'} + \mathrm{V}_{\mathrm{O}}^{\bullet\bullet} + 1/2\mathrm{O}_2 \quad (4)$$

Here, $\mathrm{Ce}_{\mathrm{Ce}}^{'}$ ions can be represented as electrons localized at the Ce-cations, $\mathrm{Ce}_{\mathrm{Ce}}^{'} \equiv \{\mathrm{Ce}_{\mathrm{Ce}}^{\times} + e^{'}\}$. As a consequence, the OCV values of $CeO_2$-based SOFCs and SOECs are considerably lower (by 100–300 mV at 600–800 °C) than the theoretical values. Indeed, both ionic and electronic conductivities become to be equal at $pO_2$ equal to $1.0 \times 10^{-24}$, $1.0 \times 10^{-20}$, and $2.5 \times 10^{-17}$ atm at 600, 700, and 800 °C, respectively (Fig. 9b).[157] These $pO_2$ values fall within a range of the experimentally achieved conditions. As an example, the $pO_2$ values in 3%$H_2O$ in $H_2$ (which is often used as a fuel) are $1.3 \times 10^{-27}$, $1.4 \times 10^{-24}$, and $4.3 \times 10^{-22}$ atm at 600, 700, and 800 °C, respectively. It can therefore be concluded that the electronic conductivity of $CeO_2$-based materials is greater than that of the oxygen-ionic one in 3% $H_2O/H_2$.

The non-ionic transfer of doped ceria materials results not only in lower OCVs, but also in an internal short-circuit effect caused by the appearance of electronic leakage current (ELC) in the electrolyte layer. The latter significantly reduces the energy and faradaic efficiencies of the corresponding electrochemical cells. If the ELC is somewhat reduced with increasing load in $CeO_2$-based SOFCs (Fig. 9c),[158] the ELC values become exceedingly high for SOEC operation, particularly with increasing current density. This is a primary reason why such electrolytes are not employed for high-temperature steam or carbon dioxide electrolysis.

Sections 3.5–3.7 highlight the basic information on cerates, zirconates, and cerate-zirconates. Their transport properties, as well as other representatives of proton-conducting oxides, are very similar to each other and are discussed in brief below.

Protons are not are not intrinsic defects of origin complex oxides. Protons appear in their structure during the interaction of such oxides with hydrogen-containing atmospheres at elevated temperatures. Steam of a gas media represents one of the most common sources of protons:

$$\mathrm{H_2O} + \mathrm{V}_{\mathrm{O}}^{\bullet\bullet} + \mathrm{O}_{\mathrm{O}}^{\times} \rightleftarrows 2\mathrm{OH}_{\mathrm{O}}^{\bullet} \quad (5)$$

As can be observed, a prerequisite for proton formation is the presence of oxygen vacancies, which can be filled with water molecules (a process known as dissociative adsorption of water vapor). While oxygen vacancies also exist in stabilized $ZrO_2$ and doped $CeO_2/LaGaO_3$, these phases do not exhibit any signs of hydration. In other words, a particular set of chemical and crystal structure characteristics must be met to achieve optimal phase hydration coupled with a high proton concentration. Low electronegativity of atoms, large cations, ability to form large and symmetrical crystal structures, high cationic tolerance towards the variation of their coordination environment are some of these characteristics.[98]

Because they contain both oxygen vacancies and proton defects, proton-conducting oxides can exhibit either oxygen-ionic or protonic conductivity, the dominance of which depends on the external parameters.[57] In the case of humidification of the atmosphere and a decrease in temperature, the vast majority of oxygen vacancies are occupied by water molecules, resulting in a high proton concentration in the oxides (Fig. 9d).[159] In turn, the latter become to be predominant proton conductors. When temperature increases or humid atmospheres are replaced with more dried ones, the material dehydrates, resulting in a decrease of proton concentration (according to a power low of $\sigma_{\mathrm{H}} \sim [\mathrm{OH}_{\mathrm{O}}^{\bullet}] \sim (p\mathrm{H_2O})^{1/2}$, where $pH_2O$ is the water vapor partial pressure) and a simultaneous increase of oxygen vacancy concentration (eqn (5)). Consequently, the oxygen-ionic transport is predominant for such boundary conditions. The concentrations of oxygen vacancies and protons as well as the corresponding oxygen-ionic and protonic conductivities can be comparable in an intermediate temperature range (for example, from 600 to 900 °C as shown in Fig. 9d for $BaCe_{0.9}Y_{0.1}O_{3-\delta}$). Therefore, these materials display co-ionic (dual ionic) transport, Fig. 9e.[160] Some researchers posit that the dual ionic electrolytes are better than purely oxygen-ionic or purely protonic analogues in terms of SOFC and SOEC applications.[161–163] However, this statement seems to be incorrect. First, all proton-conducting oxides lose protons during heating, thereby becoming co-ionic conductors. In PCFC/PCEC applications, the performance and efficiency parameters always undergo a gradual change with heating, exhibiting no unusual maximum at intermediate temperatures. Second, PCFCs are able to achieve higher OCV (Fig. 9f)[164] and efficiency (Fig. 9g)[165] values compared to those of the conventional SOFCs.

Along with co-ionic nature, many representatives of proton-conducting electrolytes also exhibit the p-type electronic conductivity under oxidizing conditions and elevated temperatures (eqn (2)). This non-ionic component of conductivity also decreases the energy efficiency of PCFCs and PCECs (Fig. 9h).[166] Features of electronic transport in such systems, possible ways of its minimization as well as methods of separating the total conductivity onto partial components were thoroughly discussed recently. This information can be found in reviews of Zvonareva *et al.*[57] and Huang *et al.*[113]

## 4 Ionic conductivity of solid oxide electrolytes as a part of SOFCs and SOECs

### 4.1. Comparison of the conductivities for massive and thin-film electrolytes

Section 3 addresses the transport properties of electrolyte materials when considered as individual dense (bulk) ceramic materials. However, the actual conductivity of the same electrolytes in solid oxide electrochemical cells is consistently lower due to the following potential effects:

(1) The ohmic resistance of an electrolyte (or its thin-film conductivity) is measured under fuel cell or electrolysis cell conditions when the cathode and anode gases create high gradients of oxygen and hydrogen partial pressures. In contrast, the conductivity of dense ceramics is determined under a specific gas atmosphere. This is of particular importance for electrolytes with different conductivities in oxidizing and reducing atmospheres.

(2) The ohmic-type resistance contribution of an electrolyte/electrode interface is negligible in conductivity measurements of bulk materials, as the majority of the resistance is attributed to the electrolyte body (eqn (6)). In contrast, for a thin-film electrolyte, the ohmic resistance is relatively low in absolute terms. Consequently, the ohmic-type resistance contribution of the electrolyte/electrode interface becomes discernible, contributing to the apparent ohmic resistance (eqn (7)). This apparent contribution is particularly pronounced in the presence of interface reactions accompanied by the formation of low-conductivity impurity phases (eqn (8)).

$$\sigma_{\text{ceramic}} = \frac{h}{(R_{\text{el}} + R_{\text{int}}) \cdot S} \overset{R_{\text{el}} \gg R_{\text{int}}}{=} \frac{h}{R_{\text{el}} \cdot S} \tag{6}$$

$$\sigma_{\text{thin-film}} = \frac{h}{(R_{\text{el}} + R_{\text{int}}) \cdot S} \overset{R_{\text{el}} \sim R_{\text{int}}}{\Rightarrow} \sigma_{\text{thin-film}}^{\text{apparent}} = \frac{h}{R_{\text{el}}^{\text{apparent}} \cdot S} \tag{7}$$

$$\sigma_{\text{thin-film}} = \frac{h}{(R_{\text{el}} + R_{\text{ip}}) \cdot S} \overset{R_{\text{el}} \sim R_{\text{ip}}}{\Rightarrow} \sigma_{\text{thin-film}}^{\text{apparent}} = \frac{h}{R_{\text{el}}^{\text{apparent}} \cdot S} \tag{8}$$

Here, $\sigma_{\text{ceramic}}$ is the conductivity of massive ceramic samples, $\sigma_{\text{thin-film}}$ is the conductivity of the thin-film electrolyte calculated on the basis of its ohmic resistance, $R_{\text{el}}$ is the true ohmic resistance of the electrolyte, $R_{\text{int}}$ is the ohmic-type resistance of the electrolyte/electrode interfaces, $R_{\text{ip}}$ is the ohmic-type resistance of the interfaces with impurity phases, the term 'apparent' means that the determined/calculated values differ from the true values, $h$ is the distance between electrodes, and $S$ is the cross-sectional area.

(3) In addition to interfacial phenomena, cation diffusion from electrodes into electrolytes is also possible. For instance, during co-sintering, nickel ions readily diffuse from Ni-based cermets to proton-conducting $BaM_{1-x}Y_xO_{3-\delta}$ perovskites ($M =$ Ce, Zr, Ce/Zr, Hf), forming a $BaY_2NiO_5$ impurity phase along the grain boundaries of the electrolyte layer.[167–169] This impurity impedes proton transport within the electrolyte, resulting in increased ohmic resistance.

In light of the aforementioned considerations, it is rational to examine the ionic conductivity of electrolytes within the context of their role in multilayered structures subjected to both oxidizing and reducing atmospheres at elevated temperatures.

The electrolyte thin-film conductivity discussed below was calculated from the electrochemical impedance spectroscopy data of SOFCs or SOECs under OCV conditions. In detail, the ohmic part of the total cell resistance (in case of its availability) was extracted at certain temperatures and then used for the calculation of the apparent thin-film conductivity, taking the electrolyte thickness and electrode surface into account (eqn (7) and **(8)**).

### 4.2. Thin-film conductivity of electrolytes

Fig. 10a and b shows the thin-film conductivities of different electrolyte classes obtained for SOFC/SOEC operating conditions in an intermediate temperature range covering 200 °C, *i.e.*, from 500 to 700 °C (see Table S1,† ref. 170–268). It should be noted that for two $ZrO_2$ families (YSZ and ScSZ), no data were provided at 500 °C. Although some papers present the performance of zirconia-based SOFCs/SOECs at such a low temperature, we did not find the corresponding electrochemical impedance spectra at 500 °C. This makes direct calculation of ohmic resistance difficult.

Analyzing these data at 500–700 °C, it can be seen that the thin-film conductivity tends to increase in the following order: BZY – YSZ – ScSZ – BCZYYb – SDC/GDC – LSGM. It is very surprising that the doped $BaZrO_3$ thin-films exhibit the lowest

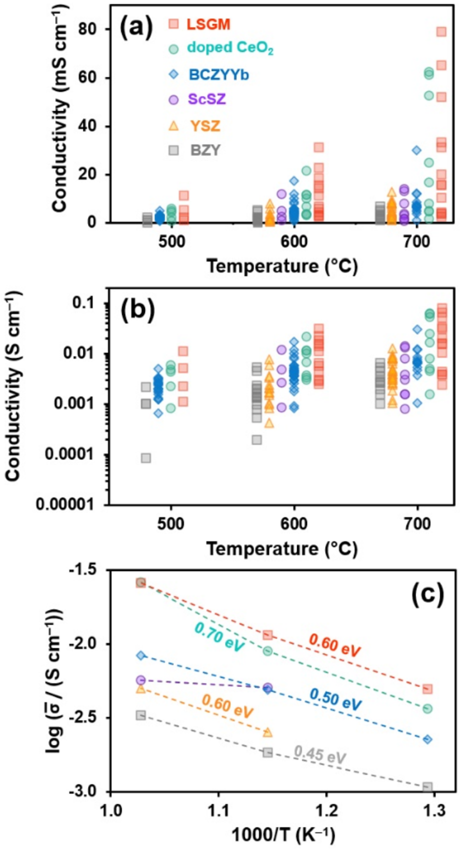

Fig. 10 Thin-film conductivity of the oxygen-ionic and proton-conducting electrolytes under SOFC or SOEC operation plotted in different coordinates (a and b). These values were calculated from the data shown in Table S1.† The panel (c) represents the temperature dependences of the average thin-film conductivity values.

conductivity among the materials in this sequence, despite their high performance in a series of massive ceramic electrolytes (Fig. 1a, b, e and f), particularly at temperatures below 700 °C. A similar situation occurs for the BCZYYb electrolytes: their thin-film conductivities are predictably higher than those of BZY, but at the same time lower compared to the thin-film conductivities of SDC, GDC, and LSGM. This also contradicts with the relative positions of the massive ceramic electrolytes at 500–600 °C. The revealed inconsistency may be attributed to different factors discussed in Section 4.1.

The thin-film conductivities of yttria and scandia stabilized zirconia electrolytes are nearly identical, occupying an intermediate position between the BZY and BCZYYb proton-conducting electrolytes. This suggests that both YSZ and ScSZ exhibit comparable transport properties in real SOFC/SOEC operation, despite their conductivity differences by 0.5–1 orders of magnitude for the massive samples (Fig. 1b and c).

A comparison of two remaining oxygen-ionic classes reveals that the thin-film conductivities of gallate electrolytes are close to those of ceria electrolytes, with some exceptions. These exceptions can be explained by the fact that very high thin-film conductivity values were obtained for rather thick gallate electrolytes (see Table S1†). According to eqn (6), the ohmic resistance of a thick electrolyte is much higher than the ohmic-type resistance of the electrolyte/electrode interfaces. As a result, the calculated conductivity is not biased by interfacial processes and achieves superior levels compared to SOFCs/SOECs with thinner electrolytes.

Fig. 10c compares the average values of thin-film conductivities in the Arrhenius coordinates. Prior to discussing behaviors, it should be noted that the data for the ScSZ electrolyte are limited by several sources, which precludes the accurate calculation of the activation energy ($E_a$) values. As can be seen, these average values align with the recently revealed sequence of BZY – YSZ – ScSZ – BCZYYb – SDC/GDC – LSGM.

## 5 Conclusions

This work revisits the ionic conductivity of state-of-the-art SOFC and SOEC electrolytes, considering their diverse forms, including massive ceramic samples and thin-film layers. This endeavor was driven by the motivation to update the classical, yet somewhat outdated, dependencies (Fig. 1) on which the conductivities of widely studied electrolytes are compared with each other.

First, a dataset of at least 10 dependences for each electrolyte class was obtained and plotted to demonstrate the possible window of conductivity variation. As can be seen from the comparative analysis presented in Fig. 2–8, the differences in total conductivity of the same (or close) materials attain ~1 order of magnitude for YSZ and increase up to 3 orders of magnitude for proton-conducting materials at low temperatures. The same behavior is observed for thin-film electrolytes, whose conductivity can vary in a range of two orders of magnitude (Fig. 10). There are common factors that explain the revealed differences, including microstructural parameters such as relative density, porosity, grain size, and uncontrolled or technologically introduced impurities. In addition, each electrolyte class exhibits specific properties (Scheme 1), which can significantly impair the ionic transport of massive or thin-film ceramic materials. These chemical and electrochemical aspects must be considered during the rational design of highly conductive electrolytes.

A combined consideration of the selected conductivities for different electrolytes in different forms allows a revised graph to be plotted, as shown in Fig. 11. In the case of dense massive

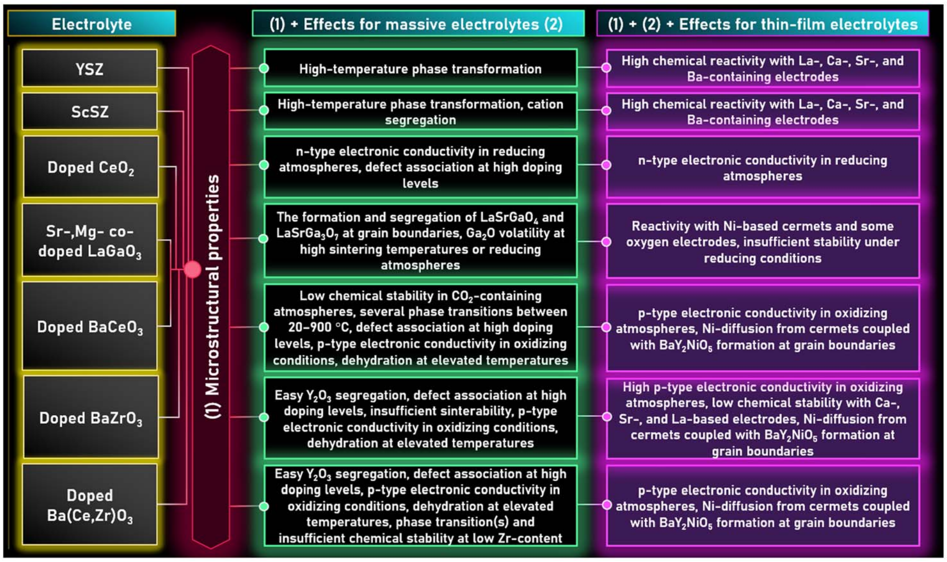

| Electrolyte | (1) + Effects for massive electrolytes (2) | (1) + (2) + Effects for thin-film electrolytes |
|---|---|---|
| YSZ | High-temperature phase transformation | High chemical reactivity with La-, Ca-, Sr-, and Ba-containing electrodes |
| ScSZ | High-temperature phase transformation, cation segregation | High chemical reactivity with La-, Ca-, Sr-, and Ba-containing electrodes |
| Doped $CeO_2$ | n-type electronic conductivity in reducing atmospheres, defect association at high doping levels | n-type electronic conductivity in reducing atmospheres |
| Sr-,Mg- co-doped $LaGaO_3$ | The formation and segregation of $LaSrGaO_4$ and $LaSrGa_3O_7$ at grain boundaries, $Ga_2O$ volatility at high sintering temperatures or reducing atmospheres | Reactivity with Ni-based cermets and some oxygen electrodes, insufficient stability under reducing conditions |
| Doped $BaCeO_3$ | Low chemical stability in $CO_2$-containing atmospheres, several phase transitions between 20–900 °C, defect association at high doping levels, p-type electronic conductivity in oxidizing conditions, dehydration at elevated temperatures | p-type electronic conductivity in oxidizing atmospheres, Ni-diffusion from cermets coupled with $BaY_2NiO_5$ formation at grain boundaries |
| Doped $BaZrO_3$ | Easy $Y_2O_3$ segregation, defect association at high doping levels, insufficient sinterability, p-type electronic conductivity in oxidizing conditions, dehydration at elevated temperatures | High p-type electronic conductivity in oxidizing atmospheres, low chemical stability with Ca-, Sr-, and La-based electrodes, Ni-diffusion from cermets coupled with $BaY_2NiO_5$ formation at grain boundaries |
| Doped $Ba(Ce,Zr)O_3$ | Easy $Y_2O_3$ segregation, defect association at high doping levels, p-type electronic conductivity in oxidizing conditions, dehydration at elevated temperatures, phase transition(s) and insufficient chemical stability at low Zr-content | p-type electronic conductivity in oxidizing atmospheres, Ni-diffusion from cermets coupled with $BaY_2NiO_5$ formation at grain boundaries |

Scheme 1 Possible effects (along with microstructural properties (1)) causing the considerable conductivity variation for the same or similar electrolyte materials.

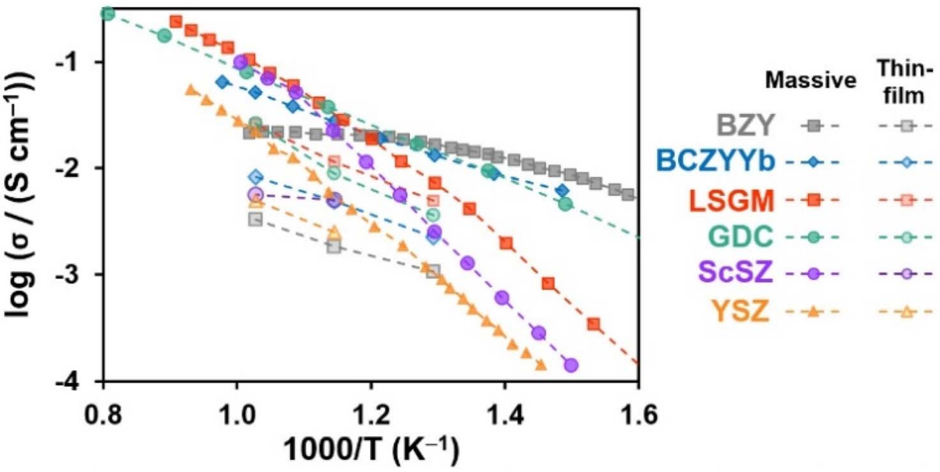

Fig. 11 A combined representation of the ionic conductivity for massive and thin-film electrolytes. From Fig. 2–8, the highest ionic conductivity for each electrolyte class was presented here.

ceramics, the obtained behaviors are typically close to the data presented in Fig. 1a, b and f, including the absolute conductivity values and electrolyte positions relative to each other. It is noteworthy that at temperatures above 600 °C, the maximal conductivity differences for the considered materials do not exceed one order of magnitude, while these differences amount to approximately two orders of magnitude at lower temperatures. This indicates that the electrical properties of the ceramics are strongly dependent on their microstructural features, especially at low temperatures, when grain boundary transport has a considerable contribution to the overall conductivity. Therefore, the grain boundary processes associated with element segregation or impurity formation become prominent.

It is important to reiterate that the ionic conductivity of each electrolyte under fuel cell or electrolysis cell operation (separated gas spaces) is considerably lower than that of the massive samples measured under unseparated gas spaces. For instance, doped $BaZrO_3$ electrolytes, characterized by the highest conductivity among massive ceramics, exhibit the lowest ionic conductivity for the thin-film electrolyte series. A number of factors, including interface processes and transport variability for Ox/Red conditions, are responsible for this discrepancy. Interestingly, the doped LSGM materials exhibit the smallest conductivity differences between the massive and thin-film forms.

This work focuses on the most popular fluorite and perovskite oxides, which exhibit high ionic transport. However, there are numerous other promising electrolytes with diverse structural types[85,269–274] that are not included in this analysis. This limitation is based on the fact that alternative analogues have been insufficiently or fragmentarily studied, preventing, for example, the acquisition of a similar conductivity dataset from 10 independent sources. Nevertheless, these electrolytes continue to be researched to solve various problems in fundamental and technological areas.

## Data availability

No new data were generated as part of this review.

## Author contributions

D. E. Matkin: investigation, data curation, resources, formal analysis, writing – original draft. I. A. Starostina: investigation, methodology, validation, visualization, writing – original draft. M. B. Hanif: formal analysis, investigation, writing – original draft. D. A. Medvedev: conceptualization, data curation, project administration, writing – original draft, writing – review & editing.

## Conflicts of interest

There are no conflicts to declare.

## Acknowledgements

This work was prepared within the framework of the budgetary plans of the Hydrogen Energy Laboratory (Ural Federal University) and Institute of High Temperature Electrochemistry.

## References

1 S. Baratov, E. Filonova, A. Ivanova, M. B. Hanif, M. Irshad, M. Z. Khan, M. Motola, S. Rauf and D. Medvedev, *J. Energy Chem.*, 2024, **94**, 302, DOI: **10.1016/j.jechem.2024.02.047**.
2 A. H. Alaedini, H. K. Tourani and M. Saidi, *J. Environ. Manag.*, 2023, **329**, 117077, DOI: **10.1016/j.jenvman.2022.117077**.
3 S. E. Wolf, F. E. Winterhalder, V. Vibhu, L. G. J. B. de Haart, O. Guillon, R. A. Eichel and N. H. Menzler, *J. Mater. Chem. A*, 2023, **11**, 17977, DOI: **10.1039/D3TA02161K**.
4 L. A. Jolaoso, I. T. Bello, O. A. Ojelade, A. Yousuf, C. Duan and P. Kazempoor, *Int. J. Hydrogen Energy*, 2023, **48**, 33017, DOI: **10.1016/j.ijhydene.2023.05.077**.
5 Y. Li, L. Zhang, B. Yu, J. Zhu and C. Wu, *Engineering*, 2023, **21**, 101, DOI: **10.1016/j.eng.2022.02.016**.

6 D. Tang, G. L. Tan, G. W. Li, J. G. Liang, S. M. Ahmad, A. Bahadur, M. Humayun, H. Ullah, A. Khan and M. Bououdina, *J. Energy Storage*, 2023, **64**, 107196, DOI: 10.1016/j.est.2023.107196.

7 W. Zhang, M. Liu, X. Gu, Y. Shi, Z. Deng and N. Cai, *Chem. Rev.*, 2023, **123**, 7119, DOI: 10.1021/acs.chemrev.2c00573.

8 A. G. Elkafas, M. Rivarolo, E. Gadducci, L. Magistri and A. F. Massardo, *Processes*, 2022, **11**, 97, DOI: 10.3390/pr11010097.

9 B. S. Zainal, P. J. Ker, H. Mohamed, H. C. Ong, I. M. R. Fattah, S. M. A. Rahman, L. D. Nghiem and T. M. I. Mahlia, *Renew. Sustain. Energy Rev.*, 2024, **189**, 113941, DOI: 10.1016/j.rser.2023.113941.

10 M. B. Hossain, M. R. Islam, K. M. Muttaqi, D. Sutanto and A. P. Agalgaonkar, *J. Energy Storage*, 2023, **62**, 106842, DOI: 10.1016/j.est.2023.106842.

11 M. C. Williams, S. D. Vora and G. Jesionowski, *ECS Trans.*, 2020, **96**, 1, DOI: 10.1149/09601.0001ecst.

12 Y. Wang, J. Shi, X. Gu, O. Deutschmann, Y. Shi and N. Cai, *Prog. Energy Combust. Sci.*, 2024, **102**, 101141, DOI: 10.1016/j.pecs.2023.101141.

13 V. Cigolotti, M. Genovese and P. Fragiacomo, *Energies*, 2021, **14**, 4963, DOI: 10.3390/en14164963.

14 D. Udomsilp, C. Lenser, O. Guillon and N. H. Menzler, *Energy Technol.*, 2021, **9**, 2001062, DOI: 10.1002/ente.202001062.

15 J. Schefold, H. Poepke and A. Brisse, *ECS Trans.*, 2020, **97**, 553, DOI: 10.1149/09707.0553ecst.

16 Q. Fang, L. Blum and D. Stolten, *J. Electrochem. Soc.*, 2019, **166**, F1320, DOI: 10.1149/2.0751916jes.

17 Q. Fang, L. Blum and D. Stolten, *ECS Trans.*, 2019, **91**, 687, DOI: 10.1149/09101.0687ecst.

18 P. Piccardo, R. Spotorno and C. Geipel, *Energies*, 2022, **15**, 3548, DOI: 10.3390/en15103548.

19 M. Linder, T. Hocker, L. Holzer, K. A. Friedrich, B. Iwanschitz, A. Mai and J. A. Schuler, *J. Power Sources*, 2013, **243**, 508, DOI: 10.1016/j.jpowsour.2013.05.200.

20 Z. Gao, L. V. Mogni, E. C. Miller, J. G. Railsback and S. A. Barnett, *Energy Environ. Sci.*, 2016, **9**, 1602, DOI: 10.1039/C5EE03858H.

21 Y. Zhang, R. Knibbe, J. Sunarso, Y. Zhong, W. Zhou, Z. Shao and Z. Zhu, *Adv. Mater.*, 2017, **29**, 1700132, DOI: 10.1002/adma.201700132.

22 N. Mahato, A. Banerjee, A. Gupta, S. Omar and K. Balani, *Prog. Mater. Sci.*, 2015, **72**, 141, DOI: 10.1016/j.pmatsci.2015.01.001.

23 M. S. Khan, S. B. Lee, R. H. Song, J. W. Lee, T. H. Lim and S. J. Park, *Ceram. Int.*, 2016, **42**, 35, DOI: 10.1016/j.ceramint.2015.09.006.

24 K. Chen and S. P. Jiang, *J. Electrochem. Soc.*, 2016, **163**, F3070, DOI: 10.1149/2.0101611jes.

25 Y. Wang, W. Li, L. Ma, W. Li and X. Liu, *J. Mater. Sci. Technol.*, 2020, **55**, 35, DOI: 10.1016/j.jmst.2019.07.026.

26 M. S. Khan, X. Xu, R. Knibbe and Z. Zhu, *Renew. Sustain. Energy Rev.*, 2021, **143**, 110918, DOI: 10.1016/j.rser.2021.110918.

27 C. Yang, R. Guo, X. Jing, P. Li, J. Yuan and Y. Wu, *Int. J. Hydrogen Energy*, 2022, **47**, 37895, DOI: 10.1016/j.ijhydene.2022.08.240.

28 I. Sreedhar, B. Agarwal, P. Goyal and A. Agarwal, *J. Solid State Electrochem.*, 2020, **24**, 1239, DOI: 10.1007/s10008-020-04584-4.

29 J. Zhang, S. Ricote, P. V. Hendriksen and Y. Chen, *Adv. Funct. Mater.*, 2022, **32**, 2111205, DOI: 10.1002/adfm.202111205.

30 L. A. Dunyushkina, *Electrochem. Sci. Technol.*, 2022, **1**, 20221006, DOI: 10.15826/elmattech.2022.1.006.

31 M. Xu, J. Yu, Y. Song, R. Ran, W. Wang and Z. Shao, *Energy Fuels*, 2020, **34**, 10568, DOI: 10.1021/acs.energyfuels.0c02338.

32 M. Mathankumar, S. Balasubramanian, P. Hasin and J. Y. Lin, *Int. J. Hydrogen Energy*, 2024, **60**, 668, DOI: 10.1016/j.ijhydene.2024.02.170.

33 E. Kalinina and E. Pikalova, *Materials*, 2021, **14**, 5584, DOI: 10.3390/ma14195584.

34 H. Shi, C. Su, R. Ran, J. Cao and Z. Shao, *Prog. Nat. Sci.: Mater. Int.*, 2020, **30**, 764, DOI: 10.1016/j.pnsc.2020.09.003.

35 W. Zhang and Y. H. Hu, *Energy Sci. Eng.*, 2021, **9**, 984, DOI: 10.1002/ese3.886.

36 M. B. Hanif, S. Rauf, M. Motola, Z. U. D. Babar, C. J. Li and C. X. Li, *Mater. Res. Bull.*, 2022, **146**, 111612, DOI: 10.1016/j.materresbull.2021.111612.

37 T. K. Maiti, J. Majhi, S. K. Maiti, J. Singh, P. Dixit, T. Rohilla, S. Ghosh, S. Bhushan and S. Chattopadhyay, *Environ. Sci. Pollut. Res.*, 2022, **29**, 64489, DOI: 10.1007/s11356-022-22087-9.

38 S. Anirban and A. Dutta, *Int. J. Hydrogen Energy*, 2020, **45**, 25139, DOI: 10.1016/j.ijhydene.2020.06.119.

39 Y. Ling, X. Wang, Z. Ma, K. Wei, Y. Wu, M. Khan, K. Zheng, S. Shen and S. Wang, *J. Mater. Sci.*, 2020, **55**, 1, DOI: 10.1007/s10853-019-03876-z.

40 E. Y. Pikalova and E. G. Kalinina, *Russ. Chem. Rev.*, 2021, **90**, 703, DOI: 10.1070/RCR4966.

41 E. Filonova and D. Medvedev, *Nanomaterials*, 2022, **12**, 1991, DOI: 10.3390/nano12121991.

42 E. V. Gordeev and N. M. Porotnikova, *Electrochem. Sci. Technol.*, 2023, **2**, 20232022, DOI: 10.15826/elmattech.2023.2.022.

43 N. A. Danilov, I. A. Starostina, G. N. Starostin, A. V. Kasyanova, D. A. Medvedev and Z. Shao, *Adv. Energy Mater.*, 2023, **13**, 2302175, DOI: 10.1002/aenm.202302175.

44 M. A. Nur Syafkeena, M. L. Zainor, O. H. Hassan, N. A. Baharuddin, M. H. D. Othman, C. J. Tseng and N. Osman, *J. Alloys Compd.*, 2022, **918**, 165434, DOI: 10.1016/j.jallcom.2022.165434.

45 N. L. R. M. Rashid, A. A. Samat, A. A. Jais, M. R. Somalu, A. Muchtar, N. A. Baharuddin and W. N. R. Wan Isahak, *Ceram. Int.*, 2019, **45**, 6605, DOI: 10.1016/j.ceramint.2019.01.045.

46 F. J. A. Loureiro, N. Nasani, G. S. Reddy, N. R. Munirathnam and D. P. Fagg, *J. Power Sources*, 2019, **438**, 226991, DOI: 10.1016/j.jpowsour.2019.226991.

47 A. K. Nayak and A. Sasmal, *J. Clean. Prod.*, 2023, **386**, 135827, DOI: 10.1016/j.jclepro.2022.135827.

48 M. K. Hossain, R. Chanda, A. El-Denglawey, T. Emrose, M. T. Rahman, M. C. Biswas and K. Hashizume, *Ceram. Int.*, 2021, **47**, 23725, DOI: 10.1016/j.ceramint.2021.05.167.

49 C. Y. Regalado Vera, H. Ding, D. Peterson, W. T. Gibbons, M. Zhou and D. Ding, *JPhys Energy*, 2021, **3**, 032019, DOI: 10.1088/2515-7655/ac12ab.

50 H. Dai, H. Kou, H. Wang and L. Bi, *Electrochem. Commun.*, 2018, **96**, 11, DOI: 10.1016/j.elecom.2018.09.001.

51 A. Volkov, E. Gorbova, A. Vylkov, D. Medvedev, A. Demin and P. Tsiakaras, *Sens. Actuators, B*, 2017, **244**, 1004, DOI: 10.1016/j.snb.2017.01.097.

52 H. Shi, C. Su, R. Ran, J. Cao and Z. Shao, *Prog. Nat. Sci.: Mater. Int.*, 2020, **30**, 764, DOI: 10.1016/j.pnsc.2020.09.003.

53 S. Y. Gómez and D. Hotza, *Renew. Sustain. Energy Rev.*, 2016, **61**, 155, DOI: 10.1016/j.rser.2016.03.005.

54 M. Fallah Vostakola and B. Amini Horri, *Energies*, 2021, **14**, 1280, DOI: 10.3390/en14051280.

55 E. Fabbri, D. Pergolesi and E. Traversa, *Sci. Technol. Adv. Mater.*, 2010, **11**, 044301, DOI: 10.1088/1468-6996/11/4/044301.

56 H. Su and Y. H. Hu, *Chem. Eng. J.*, 2020, **402**, 126235, DOI: 10.1016/j.cej.2020.126235.

57 I. Zvonareva, X. Z. Fu, D. Medvedev and Z. Shao, *Energy Environ. Sci.*, 2021, **15**, 439, DOI: 10.1039/d1ee03109k.

58 L. Mathur, Y. Namgung, H. Kim and S. J. Song, *J. Korean Ceram. Soc.*, 2023, **60**, 614, DOI: 10.1007/s43207-023-00296-3.

59 F. Ciacchi, K. Crane and S. Badwal, *Solid State Ionics*, 1994, **73**, 49, DOI: 10.1016/0167-2738(94)90263-1.

60 B. C. H. Steele and A. Heinzel, *Nature*, 2001, **414**, 345, DOI: 10.1038/35104620.

61 J. Zhang, C. Lenser, N. H. Menzler and O. Guillon, *Solid State Ionics*, 2020, **344**, 115138, DOI: 10.1016/j.ssi.2019.115138.

62 M. Hattori, Y. Takeda, Y. Sakaki, A. Nakanishi, S. Ohara, K. Mukai, J. H. Lee and T. Fukui, *J. Power Sources*, 2004, **126**, 23, DOI: 10.1016/j.jpowsour.2003.08.018.

63 C. Ahamer, A. K. Opitz, G. M. Rupp and J. Fleig, *J. Electrochem. Soc.*, 2017, **164**, F790, DOI: 10.1149/2.0641707jes.

64 F. Yang, H. Fang, Q. Hu, C. Zhao, X. Qian and C. Zhao, *Int. J. Electrochem. Sci.*, 2017, **12**, 8295, DOI: 10.20964/2017.09.21.

65 O. Yamamoto, *Electrochim. Acta*, 2000, **45**, 2423, DOI: 10.1016/S0013-4686(00)00330-3.

66 C. Zhang, C. J. Li, G. Zhang, X. J. Ning, C. X. Li, H. Liao and C. Coddet, *Mater. Sci. Eng., B*, 2007, **137**, 24, DOI: 10.1016/j.mseb.2006.10.005.

67 A. O. Zhigachev, V. V. Rodaev, D. V. Zhigacheva, N. V. Lyskov and M. A. Shchukina, *Ceram. Int.*, 2021, **47**, 32490, DOI: 10.1016/j.ceramint.2021.08.285.

68 J. Tan, Y. Su, T. Hu, Q. Yu, R. Tursun, Q. Li and Y. Xi, *Solid State Ionics*, 2016, **292**, 22, DOI: 10.1016/j.ssi.2016.03.018.

69 Y. Arachi, *Solid State Ionics*, 1999, **121**, 133, DOI: 10.1016/S0167-2738(98)00540-2.

70 S. Badwal, *Solid State Ionics*, 2000, **136–137**, 91, DOI: 10.1016/S0167-2738(00)00356-8.

71 J. T. S. Irvine, T. Politova, N. Zakowsky, A. Kruth, S. Tao, R. Travis and O. Attia, *NATO Sci. Ser.*, 2006, vol. 202, p. 35, DOI: 10.1007/1-4020-3498-9_4.

72 N. A. Arifin, A. A. Afifi, A. Samreen, R. S. R. M. Hafriz and A. Muchtar, *Solid State Ionics*, 2023, **399**, 116302, DOI: 10.1016/j.ssi.2023.116302.

73 M. Coduri, S. Checchia, M. Longhi, D. Ceresoli and M. Scavini, *Front. Chem.*, 2018, **6**, 526, DOI: 10.3389/fchem.2018.00526.

74 M. V. Erpalov, A. P. Tarutin, N. A. Danilov, D. A. Osinkin and D. A. Medvedev, *Russ. Chem. Rev.*, 2023, **92**, RCR5097, DOI: 10.59761/RCR5097.

75 M. Z. Khan, R. H. Song, M. T. Mehran, S. B. Lee and T. H. Lim, *Ceram. Int.*, 2021, **47**, 5839, DOI: 10.1016/j.ceramint.2020.11.002.

76 J. Koettgen, S. Grieshammer, P. Hein, B. O. H. Grope, M. Nakayama and M. Martin, *Phys. Chem. Chem. Phys.*, 2018, **20**, 14291, DOI: 10.1039/C7CP08535D.

77 M. J. D. Rushton and A. Chroneos, *Sci. Rep.*, 2014, **4**, 6068, DOI: 10.1038/srep06068.

78 D. Marrocchelli, S. R. Bishop, H. L. Tuller and B. Yildiz, *Adv. Funct. Mater.*, 2012, **22**, 1958, DOI: 10.1002/adfm.201102648.

79 H. L. Tuller and S. R. Bishop, *Annu. Rev. Mater. Res.*, 2011, **41**, 369, DOI: 10.1146/annurev-matsci-062910-100442.

80 G. Accardo, C. Ferone and R. Cioffi, *Energy Technol.*, 2016, **4**, 409, DOI: 10.1002/ente.201500275.

81 G. Kim, N. Lee, K. B. Kim, B. K. Kim, H. Chang, S. J. Song and J. Y. Park, *Int. J. Hydrogen Energy*, 2013, **38**, 1571, DOI: 10.1016/j.ijhydene.2012.11.044.

82 E. Y. Pikalova, A. A. Murashkina, V. I. Maragou, A. K. Demin, V. N. Strekalovsky and P. E. Tsiakaras, *Int. J. Hydrogen Energy*, 2011, **36**, 6175, DOI: 10.1016/j.ijhydene.2011.01.132.

83 G. B. Jung, T. J. Huang and C. L. Chang, *J. Solid State Electrochem.*, 2002, **6**, 225, DOI: 10.1007/s100080100238.

84 A. V. Kasyanova, A. O. Rudenko, Y. G. Lyagaeva and D. A. Medvedev, *Membr. Membr. Technol.*, 2021, **3**, 73, DOI: 10.1134/S2517751621020050.

85 X. Yang, A. J. Fernández-Carrión and X. Kuang, *Chem. Rev.*, 2023, **123**, 9356, DOI: 10.1021/acs.chemrev.2c00913.

86 M. Morales, J. J. Roa, J. Tartaj and M. Segarra, *J. Eur. Ceram. Soc.*, 2016, **36**, 1, DOI: 10.1016/j.jeurceramsoc.2015.09.025.

87 X. Gao, T. Liu, J. Yu and L. Li, *Ceram. Int.*, 2017, **43**, 6329, DOI: 10.1016/j.ceramint.2017.02.040.

88 J. Kim, *Solid State Ionics*, 2001, **140**, 105, DOI: 10.1016/S0167-2738(01)00687-7.

89 T. Ishihara, H. Matsuda and Y. Takita, *J. Am. Chem. Soc.*, 1994, **116**, 3801, DOI: 10.1021/ja00088a016.

90 T. Ishihara, T. Shibayama, M. Honda, H. Nishiguchi and Y. Takita, *J. Electrochem. Soc.*, 2000, **147**, 1332, DOI: 10.1149/1.1393358.

91 K. Huang, R. S. Tichy and J. B. Goodenough, *J. Am. Ceram. Soc.*, 1998, **81**, 2565, DOI: 10.1111/j.1151-2916.1998.tb02662.x.

92 D. Marrero-López, M. C. Martín-Sedeño, J. Peña-Martínez, J. C. Ruiz-Morales, P. Núñez-Coello and J. R. Ramos-Barrado, *J. Am. Ceram. Soc.*, 2011, **94**, 1031, DOI: 10.1111/j.1551-2916.2010.04233.x.

93 D. D. Wei, D. F. Zhou, S. K. Xie, G. C. Yang and J. Meng, *RSC Adv.*, 2015, **5**, 103541, DOI: 10.1039/c5ra21809h.

94 S. Xu, X. Lin, B. Ge, D. Ai, J. Ma and Z. Peng, *Int. J. Appl. Ceram. Technol.*, 2019, **16**, 108, DOI: 10.1111/ijac.13048.

95 M. Morales, J. M. Pérez-Falcón, A. Moure, J. Tartaj, F. Espiell and M. Segarra, *Int. J. Hydrogen Energy*, 2014, **39**, 5451, DOI: 10.1016/j.ijhydene.2014.01.019.

96 L. Chen, D. F. Zhou, Y. Wang, X. F. Zhu and J. Meng, *Ceram. Int.*, 2017, **43**, 3583, DOI: 10.1016/j.ceramint.2016.11.195.

97 J. Song, Y. Y. Birdja, D. Pant, Z. Chen and J. Vaes, *Int. J. Miner., Metall. Mater.*, 2022, **29**, 848, DOI: 10.1007/s12613-022-2447-y.

98 N. Kochetova, I. Animitsa, D. Medvedev, A. Demin and P. Tsiakaras, *RSC Adv.*, 2016, **6**, 73222, DOI: 10.1039/C6RA13347A.

99 Z. Shi, W. Sun, Z. Wang, J. Qian and W. Liu, *ACS Appl. Mater. Interfaces*, 2014, **6**, 5175, DOI: 10.1021/am500467m.

100 J. Yin, X. Wang, J. Xu, H. Wang, F. Zhang and G. Ma, *Solid State Ionics*, 2011, **185**, 6, DOI: 10.1016/j.ssi.2010.12.018.

101 A. Radojković, M. Žunić, S. M. Savić, S. Perać, D. L. Golić, Z. Branković and G. Branković, *Ceram. Int.*, 2019, **45**, 8279, DOI: 10.1016/j.ceramint.2019.01.134.

102 S. M. Haile, G. Staneff and K. H. Ryu, *J. Mater. Sci.*, 2001, **36**, 1149, DOI: 10.1023/A:1004877708871.

103 Y. P. Fu and C. S. Weng, *Ceram. Int.*, 2014, **40**, 10793, DOI: 10.1016/j.ceramint.2014.03.069.

104 W. Suksamai and I. Metcalfe, *Solid State Ionics*, 2007, **178**, 627, DOI: 10.1016/j.ssi.2007.02.003.

105 A. Lacz, *J. Therm. Anal. Calorim.*, 2019, **138**, 4187, DOI: 10.1007/s10973-019-08147-2.

106 D. Medvedev, A. Murashkina, E. Pikalova, A. Demin, A. Podias and P. Tsiakaras, *Prog. Mater. Sci.*, 2014, **60**, 72, DOI: 10.1016/j.pmatsci.2013.08.001.

107 Y. C. Lee, I. M. Hung, S. L. Chang, C. J. Ciou and J. S. Wu, *J. Eur. Ceram. Soc.*, 2011, **31**, 3137, DOI: 10.1016/j.jeurceramsoc.2011.05.003.

108 L. He, H. Gao, Y. Xuan, F. Zhang, J. Ren and M. Chen, *Comput. Mater. Sci.*, 2022, **202**, 111007, DOI: 10.1016/j.commatsci.2021.111007.

109 F. Zhao and F. Chen, *Int. J. Hydrogen Energy*, 2010, **35**, 11194, DOI: 10.1016/j.ijhydene.2010.06.073.

110 S. Wang, J. Shen, Z. Zhu, Z. Wang, Y. Cao, X. Guan, Y. Wang, Z. Wei and M. Chen, *J. Power Sources*, 2018, **387**, 24, DOI: 10.1016/j.jpowsour.2018.03.054.

111 L. He, Y. Xuan, F. Zhang, X. Wang, H. Pan, J. Ren and M. Chen, *Int. J. Hydrogen Energy*, 2021, **46**, 1096, DOI: 10.1016/j.ijhydene.2020.09.168.

112 D. A. Medvedev, *Curr. Opin. Green Sustainable Chem.*, 2021, **32**, 100549, DOI: 10.1016/j.cogsc.2021.100549.

113 Y. Huang, R. Qiu, W. Lian, L. Lei, T. Liu, J. Zhang, Y. Wang, J. Liu, J. Huang and F. Chen, *J. Power Sources*, 2022, **528**, 231201, DOI: 10.1016/j.jpowsour.2022.231201.

114 L. Lu, Y. Liu, H. Zhang, Y. Xu and H. Chen, *J. Mater. Chem. A*, 2023, **11**, 23613, DOI: 10.1039/D3TA05035A.

115 A. V. Kasyanova, L. R. Tarutina, A. O. Rudenko, J. G. Lyagaeva and D. A. Medvedev, *Russ. Chem. Rev.*, 2020, **89**, 667, DOI: 10.1070/RCR4928.

116 M. Papac, V. Stevanović, A. Zakutayev and R. O'Hayre, *Nat. Mater.*, 2021, **20**, 301, DOI: 10.1038/s41563-020-00854-8.

117 S. A. Rasaki, C. Liu, C. Lao and Z. Chen, *Prog. Solid State Chem.*, 2021, **63**, 100325, DOI: 10.1016/j.progsolidstchem.2021.100325.

118 A. Uthayakumar, A. Pandiyan and S. B. Krishna Moorthy, *Int. J. Hydrogen Energy*, 2018, **43**, 23488, DOI: 10.1016/j.ijhydene.2018.10.185.

119 D. Han and T. Uda, *J. Mater. Chem. A*, 2018, **6**, 18571, DOI: 10.1039/C8TA06280C.

120 J. N. Ebert, D. Jennings, L. A. Schäfer, D. Sebold and W. Rheinheimer, *Scr. Mater.*, 2024, **241**, 115852, DOI: 10.1016/j.scriptamat.2023.115852.

121 A. V. Kuz'min, V. B. Balakireva, S. V. Plaksin and V. P. Gorelov, *Russ. J. Electrochem.*, 2009, **45**, 1351, DOI: 10.1134/S1023193509120064.

122 M. François, V. Lescure, O. Heintz, L. Combemale, F. Demoisson and G. Caboche, *Ceram. Int.*, 2023, **49**, 25344, DOI: 10.1016/j.ceramint.2023.05.070.

123 C. Y. Yoo, D. S. Yun, J. H. Joo and J. H. Yu, *J. Alloys Compd.*, 2015, **621**, 263, DOI: 10.1016/j.jallcom.2014.09.207.

124 M. Irshad, Q. Ain, K. Siraj, R. Raza, A. N. Tabish, M. Rafique, R. Idrees, F. Khan, S. Majeed and M. Ahsan, *J. Alloys Compd.*, 2020, **815**, 152389, DOI: 10.1016/j.jallcom.2019.152389.

125 L. Ge, J. Jiao, Z. zhu, Q. Zhang, Y. Zheng, H. Chen and L. Guo, *Ceram. Int.*, 2019, **45**, 24946, DOI: 10.1016/j.ceramint.2019.08.202.

126 Z. Zhu and S. Wang, *Ceram. Int.*, 2019, **45**, 19289, DOI: 10.1016/j.ceramint.2019.06.179.

127 H. Shimada, X. Li, A. Hagiwara and M. Ihara, *J. Electrochem. Soc.*, 2013, **160**, F597, DOI: 10.1149/2.079306jes.

128 S. Tao and J. T. S. Irvine, *J. Solid State Chem.*, 2007, **180**, 3493, DOI: 10.1016/j.jssc.2007.09.027.

129 Y. Ding, Y. LI, W. Deng, W. Huang and C. Wang, *J. Rare Earths*, 2013, **31**, 1017, DOI: 10.1016/S1002-0721(13)60023-X.

130 N. A. Danilov, J. G. Lyagaeva, D. A. Medvedev, A. K. Demin and P. Tsiakaras, *Electrochim. Acta*, 2018, **284**, 551, DOI: 10.1016/j.electacta.2018.07.179.

131 C. Duan, R. Kee, H. Zhu, N. Sullivan, L. Zhu, L. Bian, D. Jennings and R. O'Hayre, *Nat. Energy*, 2019, **4**, 230, DOI: 10.1038/s41560-019-0333-2.

132 D. Han, X. Liu, T. S. Bjørheim and T. Uda, *Adv. Energy Mater.*, 2021, **11**, 2003149, DOI: 10.1002/aenm.202003149.

133 J. Li, C. Wang, X. Wang and L. Bi, *Electrochem. Commun.*, 2020, **112**, 106672, DOI: 10.1016/j.elecom.2020.106672.

134 D. A. Medvedev, J. G. Lyagaeva, E. V. Gorbova, A. K. Demin and P. Tsiakaras, *Prog. Mater. Sci.*, 2016, **75**, 38, DOI: 10.1016/j.pmatsci.2015.08.001.

135 B. Lin, S. Zhang, L. Zhang, L. Bi, H. Ding, X. Liu, J. Gao and G. Meng, *J. Power Sources*, 2008, **177**, 330, DOI: 10.1016/j.jpowsour.2007.11.109.

136 H. Ding, B. Lin, X. Liu and G. Meng, *Electrochem. Commun.*, 2008, **10**, 1388, DOI: 10.1016/j.elecom.2008.07.016.

137 K. Xie, R. Yan, Y. Jiang, X. Liu and G. Meng, *J. Membr. Sci.*, 2008, **325**, 6, DOI: 10.1016/j.memsci.2008.07.055.

138 L. Yang, S. Wang, K. Blinn, M. Liu, Z. Liu, Z. Cheng and M. Liu, *Science*, 2009, **326**, 126, DOI: 10.1126/science.1174811.

139 Y. Liu, L. Yang, M. Liu, Z. Tang and M. Liu, *J. Power Sources*, 2011, **196**, 9980, DOI: 10.1016/j.jpowsour.2011.08.047.

140 J. Lyagaeva, G. Vdovin, L. Hakimova, D. Medvedev, A. Demin and P. Tsiakaras, *Electrochim. Acta*, 2017, **251**, 554, DOI: 10.1016/j.electacta.2017.08.149.

141 T. Ishiyama, H. Kishimoto, K. Develos-Bagarinao, K. Yamaji, T. Yamaguchi and Y. Fujishiro, *Inorg. Chem.*, 2017, **56**, 11876, DOI: 10.1021/acs.inorgchem.7b01875.

142 N. Nasani, Z. Shakel, F. J. A. Loureiro, B. B. Panigrahi, B. B. Kale and D. P. Fagg, *J. Alloys Compd.*, 2021, **862**, 158640, DOI: 10.1016/j.jallcom.2021.158640.

143 Y. Gou, Y. Zhao, J. Zhang, W. Sun, J. Qiao, K. Sun and Z. Wang, *Ceram. Int.*, 2022, **48**, 35108, DOI: 10.1016/j.ceramint.2022.08.106.

144 Y. Meng, J. Gao, H. Huang, M. Zou, J. Duffy, J. Tong and K. S. Brinkman, *J. Power Sources*, 2019, **439**, 227093, DOI: 10.1016/j.jpowsour.2019.227093.

145 A. Uthayakumar, M. Kavithanjali, K. Sandhya, N. Ponpandian and K. S. Babu, *J. Alloys Compd.*, 2021, **864**, 158098, DOI: 10.1016/j.jallcom.2020.158098.

146 K. H. Ryu and S. M. Haile, *Solid State Ionics*, 1999, **125**, 355, DOI: 10.1016/S0167-2738(99)00196-4.

147 E. Fabbri, A. Depifanio, E. Dibartolomeo, S. Licoccia and E. Traversa, *Solid State Ionics*, 2008, **179**, 558, DOI: 10.1016/j.ssi.2008.04.002.

148 Y. Guo, Y. Lin, R. Ran and Z. Shao, *J. Power Sources*, 2009, **193**, 400, DOI: 10.1016/j.jpowsour.2009.03.044.

149 D. Medvedev, J. Lyagaeva, S. Plaksin, A. Demin and P. Tsiakaras, *J. Power Sources*, 2015, **273**, 716, DOI: 10.1016/j.jpowsour.2014.09.116.

150 K. Singh, A. K. Baral and V. Thangadurai, *J. Am. Ceram. Soc.*, 2016, **99**, 866, DOI: 10.1111/jace.14008.

151 K. Singh, R. Kannan and V. Thangadurai, *Int. J. Hydrogen Energy*, 2016, **41**, 13227, DOI: 10.1016/j.ijhydene.2016.05.089.

152 G. Zhou, Y. Li, Y. Luo, X. Wang and Y. Ding, *J. Alloys Compd.*, 2024, **971**, 172668, DOI: 10.1016/j.jallcom.2023.172668.

153 Z. U. D. Babar, M. B. Hanif, M. K. Butt, M. Motola and C. X. Li, *Ceram. Int.*, 2024, **50**, 40261, DOI: 10.1016/j.ceramint.2024.03.339.

154 J. H. Park and R. N. Blumenthal, *J. Electrochem. Soc.*, 1989, **136**, 2867, DOI: 10.1149/1.2096302.

155 Y. Xiong, K. Yamaji, N. Sakai, H. Negishi, T. Horita and H. Yokokawa, *J. Electrochem. Soc.*, 2001, **148**, E489, DOI: 10.1149/1.1417977.

156 T. Kawada, *Solid State Ionics*, 1992, **53–56**, 418, DOI: 10.1016/0167-2738(92)90409-I.

157 T. Matsui, M. Inaba, A. Mineshige and Z. Ogumi, *Solid State Ionics*, 2005, **176**, 647, DOI: 10.1016/j.ssi.2004.10.011.

158 R. T. Leah, N. P. Brandon and P. Aguiar, *J. Power Sources*, 2005, **145**, 336, DOI: 10.1016/j.jpowsour.2004.12.067.

159 A. Løken, T. S. Bjørheim and R. Haugsrud, *J. Mater. Chem. A*, 2015, **3**, 23289, DOI: 10.1039/C5TA04932F.

160 F. J. A. Loureiro, D. Pérez-Coll, V. C. D. Graça, S. M. Mikhalev, A. F. G. Ribeiro, A. Mendes and D. P. Fagg, *J. Mater. Chem. A*, 2019, **7**, 18135, DOI: 10.1039/C9TA04584H.

161 J. Kim, A. Jun, O. Gwon, S. Yoo, M. Liu, J. Shin, T. H. Lim and G. Kim, *Nano Energy*, 2018, **44**, 121, DOI: 10.1016/j.nanoen.2017.11.074.

162 C. Zhou, J. Sunarso, Y. Song, J. Dai, J. Zhang, B. Gu, W. Zhou and Z. Shao, *J. Mater. Chem. A*, 2019, **7**, 13265, DOI: 10.1039/C9TA03501J.

163 F. He, Z. Teng, G. Yang, C. Zhou, D. Guan, S. Chen, R. Ran, W. Wang, W. Zhou and Z. Shao, *J. Power Sources*, 2020, **460**, 228105, DOI: 10.1016/j.jpowsour.2020.228105.

164 A. Demin, P. Tsiakaras, E. Gorbova and S. Hramova, *J. Power Sources*, 2004, **131**, 231, DOI: 10.1016/j.jpowsour.2003.10.016.

165 A. Demin, *Int. J. Hydrogen Energy*, 2001, **26**, 1103, DOI: 10.1016/S0360-3199(01)00043-X.

166 L. P. Putilov, V. I. Tsidilkovski and A. K. Demin, *J. Mater. Chem. A*, 2020, **8**, 12641, DOI: 10.1039/d0ta03935g.

167 A. V. Kasyanova, I. A. Zvonareva, N. A. Tarasova, L. Bi, D. A. Medvedev and Z. Shao, *Mater. Rep.: Energy*, 2022, **2**, 100158, DOI: 10.1016/j.matre.2022.100158.

168 S. Guo, L. Jiang, Y. Li, P. Zhong, S. A. Ismail, T. Norby and D. Han, *Adv. Funct. Mater.*, 2024, **34**, 2304729, DOI: 10.1002/adfm.202304729.

169 W. Deibert, M. E. Ivanova, Y. Huang, R. Merkle, J. Maier and W. A. Meulenberg, *J. Mater. Chem. A*, 2021, **10**, 2362, DOI: 10.1039/D1TA05240C.

170 X. Wang, T. Zhang, P. Qiu, H. Qi and B. Tu, *Int. J. Hydrogen Energy*, 2024, **51**, 1136, DOI: 10.1016/j.ijhydene.2023.11.013.

171 W. Wang, X. Zhang, K. Khan, H. Wu, D. Zhang, Y. Yang, Y. Jiang and B. Lin, *Int. J. Hydrogen Energy*, 2021, **46**, 5593, DOI: 10.1016/j.ijhydene.2020.11.020.

172 H. Qi, Z. Zhao, B. Tu and M. Cheng, *J. Power Sources*, 2020, **455**, 227971, DOI: 10.1016/j.jpowsour.2020.227971.

173 Y. LI, D. CUI, H. QI, Z. ZHAO, Y. GUO and M. CHENG, *Electrochemistry*, 2020, **88**, 290, DOI: 10.5796/electrochemistry.20-00018.

174 L. Cheng, Q. Lyu, Z. Li, Y. Liu, C. Jin, N. Xu, Q. Zhong and T. Zhu, *Int. J. Appl. Ceram. Technol.*, 2023, **20**, 2341, DOI: 10.1111/ijac.14346.

175 Y. Wu, J. Sang, Z. Liu, H. Fan, B. Cao, Q. Wang, J. Yang, W. Guan, X. Liu and J. Wang, *Ceram. Int.*, 2023, **49**, 20290, DOI: 10.1016/j.ceramint.2023.03.152.

176 F. Liang, J. Yang, H. Wang and J. Wu, *Int. J. Miner., Metall. Mater.*, 2023, **30**, 1190, DOI: 10.1007/s12613-023-2620-y.

177 A. A. Solovyev, A. V. Shipilova, S. V. Rabotkin, E. A. Smolyanskiy and A. N. Shmakov, *Int. J. Hydrogen Energy*, 2022, **47**, 37967, DOI: 10.1016/j.ijhydene.2022.08.281.

178 H. Sumi, S. Takahashi, Y. Yamaguchi and H. Shimada, *J. Asian Ceram. Soc.*, 2021, **9**, 609, DOI: 10.1080/21870764.2021.1905254.

179 S. Zhou, Y. Yang, H. Chen and Y. Ling, *Ceram. Int.*, 2020, **46**, 18331, DOI: 10.1016/j.ceramint.2020.05.057.

180 G. DiGiuseppe, D. Thompson, C. Gumeci, A. M. Hussain and N. Dale, *Ionics*, 2019, **25**, 3537, DOI: 10.1007/s11581-019-02935-4.

181 D. Tian, Y. Yang, Y. Chen, X. Lu and B. Lin, *Mater. Res. Express*, 2019, **6**, 096310, DOI: 10.1088/2053-1591/ab2ee8.

182 B. H. Yun, K. J. Kim, D. W. Joh, M. S. Chae, J. J. Lee, D. Kim, S. Kang, D. Choi, S. T. Hong and K. T. Lee, *J. Mater. Chem. A*, 2019, **7**, 20558, DOI: 10.1039/c9ta09203j.

183 M. J. López-Robledo, M. A. Laguna-Bercero, A. Larrea and V. M. Orera, *J. Power Sources*, 2018, **378**, 184, DOI: 10.1016/j.jpowsour.2017.12.035.

184 Z. Lu, S. Darvish, J. Hardy, J. Templeton, J. Stevenson and Y. Zhong, *J. Electrochem. Soc.*, 2017, **164**, F3097, DOI: 10.1149/2.0141710jes.

185 B. Liang, S. Zhang, S. Lu, S. Sui and J. Shang, *Int. J. Appl. Ceram. Technol.*, 2017, **14**, 185, DOI: 10.1111/ijac.12625.

186 W. Wu, Z. Zhao, X. Zhang, Z. Liu, D. Cui, B. Tu, D. Ou and M. Cheng, *Electrochem. Commun.*, 2016, **71**, 43, DOI: 10.1016/j.elecom.2016.08.005.

187 X. Zhang, W. Wu, Z. Zhao, B. Tu, D. Ou, D. Cui and M. Cheng, *Catal. Sci. Technol.*, 2016, **6**, 4945, DOI: 10.1039/c5cy02232k.

188 J. Qian, J. Hou, Z. Tao and W. Liu, *J. Alloys Compd.*, 2015, **631**, 255, DOI: 10.1016/j.jallcom.2015.01.124.

189 C. Jeong, J. H. Lee, M. Park, J. Hong, H. Kim, J. W. Son, J. H. Lee, B. K. Kim and K. J. Yoon, *J. Power Sources*, 2015, **297**, 370, DOI: 10.1016/j.jpowsour.2015.08.023.

190 H. G. Desta, D. Tian, Q. Yang, S. Zhu, K. Song, Y. Chen and B. Lin, *Chem. Phys. Lett.*, 2022, **806**, 140037, DOI: 10.1016/j.cplett.2022.140037.

191 S. Y. Park, J. H. Ahn, C. W. Jeong, C. W. Na, R. H. Song and J. H. Lee, *Int. J. Hydrogen Energy*, 2014, **39**, 12894, DOI: 10.1016/j.ijhydene.2014.06.103.

192 J. C. Chang, M. C. Lee, R. J. Yang, Y. C. Chang, T. N. Lin, C. H. Wang, W. X. Kao and L. S. Lee, *J. Power Sources*, 2011, **196**, 3129, DOI: 10.1016/j.jpowsour.2010.12.036.

193 M. Moon, P. Guha, S. Oh, H. Jung, S. Yang, J. H. Lee, Y. Jun, J. W. Son and D. H. Kwon, *J. Power Sources*, 2024, **589**, 233774, DOI: 10.1016/j.jpowsour.2023.233774.

194 A. Hussain, M. Z. Khan, R. H. Song, J. E. Hong, S. B. Lee and T. H. Lim, *ECS Trans.*, 2019, **91**, 373, DOI: 10.1149/09101.0373ecst.

195 G. Y. Cho, Y. H. Lee, S. W. Hong, J. Bae, J. An, Y. B. Kim and S. W. Cha, *Int. J. Hydrogen Energy*, 2015, **40**, 15704, DOI: 10.1016/j.ijhydene.2015.09.124.

196 B. Huang, X. F. Ye, S. R. Wang, H. W. Nie, R. Z. Liu and T. L. Wen, *Mater. Res. Bull.*, 2007, **42**, 1705, DOI: 10.1016/j.materresbull.2006.11.027.

197 S. W. Shin, A. Hussain, M. Z. Khan, D. W. Joh, T. H. Lim, S. B. Lee, J. E. Hong, J. H. Shim and R. H. Song, *Prog. Nat. Sci.: Mater. Int.*, 2023, **33**, 733, DOI: 10.1016/j.pnsc.2023.12.012.

198 Y. Meng, H. Zheng, J. Duffy, H. Huang, K. He, J. Tong and K. S. Brinkman, *J. Power Sources*, 2023, **560**, 232724, DOI: 10.1016/j.jpowsour.2023.232724.

199 T. Yamaguchi, S. Shimizu, T. Suzuki, Y. Fujishiro and M. Awano, *J. Electrochem. Soc.*, 2008, **155**, B423, DOI: 10.1149/1.2839618.

200 H. Shi, R. Ran and Z. Shao, *Int. J. Hydrogen Energy*, 2012, **37**, 1125, DOI: 10.1016/j.ijhydene.2011.02.077.

201 T. Suzuki, B. Liang, T. Yamaguchi, H. Sumi, K. Hamamoto and Y. Fujishiro, *J. Power Sources*, 2012, **199**, 170, DOI: 10.1016/j.jpowsour.2011.10.046.

202 Q. Li, X. Wang, C. Li, X. Yang, L. Jia and J. Li, *Composites, Part B*, 2022, **229**, 109462, DOI: 10.1016/j.compositesb.2021.109462.

203 R. Song, X. Zhang, D. Huan, X. Li, N. Shi, C. Xia, R. Peng and Y. Lu, *Int. J. Hydrogen Energy*, 2023, **48**, 32943, DOI: 10.1016/j.ijhydene.2023.04.351.

204 X. Wang, W. Li, C. Zhou, M. Xu, Z. Hu, C. W. Pao, W. Zhou and Z. Shao, *ACS Appl. Mater. Interfaces*, 2023, **15**, 1339, DOI: 10.1021/acsami.2c19343.

205 P. Qiu, B. Liu, L. Wu, H. Qi, B. Tu, J. Li and L. Jia, *J. Adv. Ceram.*, 2022, **11**, 1988, DOI: 10.1007/s40145-022-0662-7.

206 S. H. Hwang, S. K. Kim, J. T. Nam and J. S. Park, *Int. J. Hydrogen Energy*, 2021, **46**, 33551, DOI: 10.1016/j.ijhydene.2021.07.179.

207 L. Zhu, R. O'Hayre and N. P. Sullivan, *Int. J. Hydrogen Energy*, 2021, **46**, 27784, DOI: 10.1016/j.ijhydene.2021.06.018.

208 Y. Meng, J. Duffy, B. T. Na, J. Gao, T. Yang, J. Tong, S. Lee and K. S. Brinkman, *Solid State Ionics*, 2021, **368**, 115639, DOI: 10.1016/j.ssi.2021.115639.

209 H. Lee, H. Jung, C. Kim, S. Kim, I. Jang, H. Yoon, U. Paik and T. Song, *ACS Appl. Energy Mater.*, 2021, **4**, 11564, DOI: 10.1021/acsaem.1c02311.

210 J. Li, J. Hou, Y. Lu, Q. Wang, X. Xi, Y. Fan, X. Z. Fu and J. L. Luo, *J. Power Sources*, 2020, **453**, 227909, DOI: 10.1016/j.jpowsour.2020.227909.

211 F. He, M. Liang, W. Wang, R. Ran, G. Yang, W. Zhou and Z. Shao, *Energy Fuels*, 2020, **34**, 11464, DOI: 10.1021/acs.energyfuels.0c02370.

212 K. Wei, N. Li, Y. Wu, W. Song, X. Wang, L. Guo, M. Khan, S. Wang, F. Zhou and Y. Ling, *Ceram. Int.*, 2019, **45**, 18583, DOI: 10.1016/j.ceramint.2019.06.081.

213 M. Shang, J. Tong and R. O'Hayre, *RSC Adv.*, 2013, **3**, 15769, DOI: 10.1039/c3ra41828f.

214 K. Leonard, M. E. Ivanova, A. Weber, W. Deibert, W. A. Meulenberg, T. Ishihara and H. Matsumoto, *Solid State Ionics*, 2022, **379**, 115918, DOI: 10.1016/j.ssi.2022.115918.

215 Y. Xu, F. Hu, Y. Guo, J. Zhang, Y. Huang, W. Zhou, J. Sun, B. He and L. Zhao, *Sep. Purif. Technol.*, 2022, **297**, 121482, DOI: 10.1016/j.seppur.2022.121482.

216 Z. Pan, C. Duan, T. Pritchard, A. Thatte, E. White, R. Braun, R. O'Hayre and N. P. Sullivan, *Appl. Catal., B*, 2022, **307**, 121196, DOI: 10.1016/j.apcatb.2022.121196.
217 Q. Zhang, Y. Hou, L. Chen, L. Wang and K. Chou, *Ceram. Int.*, 2022, **48**, 17816, DOI: 10.1016/j.ceramint.2022.03.052.
218 H. Liu, K. Zhu, Y. Liu, W. Li, L. Cai, X. Zhu, M. Cheng and W. Yang, *Electrochim. Acta*, 2018, **279**, 224, DOI: 10.1016/j.electacta.2018.05.086.
219 J. Liu, J. Ding, L. Miao, Z. Gong, K. Li and W. Liu, *J. Alloys Compd.*, 2019, **786**, 163, DOI: 10.1016/j.jallcom.2019.01.312.
220 Y. Ling, J. Yu, B. lin, X. Zhang, L. Zhao and X. Liu, *J. Power Sources*, 2011, **196**, 2631, DOI: 10.1016/j.jpowsour.2010.11.017.
221 N. Nasani, D. Ramasamy, S. Mikhalev, A. V. Kovalevsky and D. P. Fagg, *J. Power Sources*, 2015, **278**, 582, DOI: 10.1016/j.jpowsour.2014.12.124.
222 X. Yu, J. Fan and L. Xue, *Ceram. Int.*, 2014, **40**, 13627, DOI: 10.1016/j.ceramint.2014.05.089.
223 C. J. Fu, Q. L. Liu, S. H. Chan, X. M. Ge and G. Pasciak, *Int. J. Hydrogen Energy*, 2010, **35**, 11200, DOI: 10.1016/j.ijhydene.2010.07.049.
224 J. Hou, F. Liu, Z. Gong, Y. Wu and W. Liu, *J. Power Sources*, 2015, **299**, 32, DOI: 10.1016/j.jpowsour.2015.08.077.
225 H. Y. Jung, K. S. Hong, H. G. Jung, H. Kim, H. R. Kim, J. W. Son, J. Kim, H. W. Lee and J. H. Lee, *J. Electrochem. Soc.*, 2007, **154**, B480, DOI: 10.1149/1.2712131.
226 Z. Jiang, A. L. Snowdon, A. Siddiq, A. El-kharouf and R. Steinberger-Wilckens, *Ceram. Int.*, 2022, **48**, 32844, DOI: 10.1016/j.ceramint.2022.07.211.
227 T. Chen, Z. Lu, G. Zeng, Y. Xie, J. Xiao and Z. Xu, *J. Power Sources*, 2024, **591**, 233886, DOI: 10.1016/j.jpowsour.2023.233886.
228 J. Shen, G. Yang, Z. Zhang, M. O. Tadé, W. Zhou and Z. Shao, *J. Power Sources*, 2017, **342**, 644, DOI: 10.1016/j.jpowsour.2016.12.109.
229 X. Chen, J. Wang, Q. Liang, X. Sun, X. Zhu, D. Zhou and J. Meng, *Solid State Sci.*, 2020, **100**, 106108, DOI: 10.1016/j.solidstatesciences.2019.106108.
230 M. Chen, B. H. Kim, Q. Xu, B. G. Ahn and D. P. Huang, *J. Membr. Sci.*, 2010, **360**, 461, DOI: 10.1016/j.memsci.2010.05.045.
231 M. Liu, D. Ding, Y. Bai, T. He and M. Liu, *J. Electrochem. Soc.*, 2012, **159**, B661, DOI: 10.1149/2.032206jes.
232 J. Choi, B. Kim and D. Shin, *J. Eur. Ceram. Soc.*, 2013, **33**, 2269, DOI: 10.1016/j.jeurceramsoc.2013.01.015.
233 M. Liu, F. Uba and Y. Liu, *J. Am. Ceram. Soc.*, 2020, **103**, 5325, DOI: 10.1111/jace.17203.
234 J. Qian, C. Lin, Z. Chen, J. Huang, N. Ai, S. P. Jiang, X. Zhou, X. Wang, Y. Shao and K. Chen, *Appl. Catal., B*, 2024, **346**, 123742, DOI: 10.1016/j.apcatb.2024.123742.
235 Z. Yang, C. Yang, B. Xiong, M. Han and F. Chen, *J. Power Sources*, 2011, **196**, 9164, DOI: 10.1016/j.jpowsour.2011.06.096.
236 D. Han, H. Wu, J. Li, S. Wang and Z. Zhan, *J. Power Sources*, 2014, **246**, 409, DOI: 10.1016/j.jpowsour.2013.07.113.
237 S. F. Wang, H. C. Lu, Y. F. Hsu and P. Jasinski, *Int. J. Hydrogen Energy*, 2022, **47**, 5429, DOI: 10.1016/j.ijhydene.2021.11.132.
238 J. H. Joo, D. Y. Kim and G. M. Choi, *Electrochem. Solid-State Lett.*, 2009, **12**, B65, DOI: 10.1149/1.3086261.
239 L. Ma, Y. Wang, W. Li, B. Guan, H. Qi, H. Tian, L. Zhou, H. A. De Santiago and X. Liu, *J. Power Sources*, 2021, **488**, 229458, DOI: 10.1016/j.jpowsour.2021.229458.
240 Z. Tan, J. T. Song, A. Takagaki and T. Ishihara, *J. Mater. Chem. A*, 2020, **9**, 1530, DOI: 10.1039/D0TA08564B.
241 W. Wang, Z. Yang, H. Wang, G. Ma, W. Gao and Z. Zhou, *J. Power Sources*, 2011, **196**, 3539, DOI: 10.1016/j.jpowsour.2010.12.037.
242 Y. Lin and S. A. Barnett, *Electrochem. Solid-State Lett.*, 2006, **9**, A285, DOI: 10.1149/1.2191132.
243 W. Guo, J. Liu and Y. Zhang, *Electrochim. Acta*, 2008, **53**, 4420, DOI: 10.1016/j.electacta.2008.01.039.
244 Y. X. Liu, S. F. Wang, Y. F. Hsu and W. Y. Yeh, *Surf. Coat. Technol.*, 2018, **344**, 507, DOI: 10.1016/j.surfcoat.2018.03.073.
245 Y. P. Wang, J. T. Gao, J. H. Li, C. J. Li and C. X. Li, *Int. J. Hydrogen Energy*, 2021, **46**, 32655, DOI: 10.1016/j.ijhydene.2021.07.121.
246 A. R. Gilev, E. A. Kiselev and V. A. Cherepanov, *Solid State Ionics*, 2019, **339**, 115001, DOI: 10.1016/j.ssi.2019.115001.
247 J. Liu, Y. Lei, Y. Li, J. Gao, D. Han, W. Zhan, F. Huang and S. Wang, *Electrochem. Commun.*, 2017, **78**, 6, DOI: 10.1016/j.elecom.2017.02.019.
248 M. Zhang, C. Song, K. Lin, M. Liu, K. Du, K. Wen, T. Liu, J. Mao, X. Zhang, H. Liao and K. Zhou, *J. Therm. Spray Technol.*, 2024, **33**, 964, DOI: 10.1007/s11666-024-01751-1.
249 H. S. Yoo, S. Ju Kim, Y. T. Megra, J. Lee, J. W. Suk and W. Lee, *Appl. Surf. Sci.*, 2023, **639**, 158188, DOI: 10.1016/j.apsusc.2023.158188.
250 K. J. Kim, S. W. Choi, M. Y. Kim, M. S. Lee, Y. S. Kim and H. S. Kim, *J. Ind. Eng. Chem.*, 2016, **42**, 69, DOI: 10.1016/j.jiec.2016.07.041.
251 J. H. Wan, J. Q. Yan and J. B. Goodenough, *J. Electrochem. Soc.*, 2005, **152**, A1511, DOI: 10.1149/1.1943587.
252 M. Lo Faro and A. S. Aricò, *Int. J. Hydrogen Energy*, 2013, **38**, 14773, DOI: 10.1016/j.ijhydene.2013.08.122.
253 Z. Bi, B. Yi, Z. Wang, Y. Dong, H. Wu, Y. She and M. Cheng, *Electrochem. Solid-State Lett.*, 2004, **7**, A105, DOI: 10.1149/1.1667016.
254 S. P. Shafi, L. Bi, S. Boulfrad and E. Traversa, *J. Electrochem. Soc.*, 2015, **162**, F1498, DOI: 10.1149/2.0701514jes.
255 L. Bi, E. H. Da'as and S. P. Shafi, *Electrochem. Commun.*, 2017, **80**, 20, DOI: 10.1016/j.elecom.2017.05.006.
256 Y. Ma, B. He, J. Wang, M. Cheng, X. Zhong and J. Huang, *Int. J. Hydrogen Energy*, 2021, **46**, 9918, DOI: 10.1016/j.ijhydene.2020.04.282.
257 W. Sun, L. Yan, Z. Shi, Z. Zhu and W. Liu, *J. Power Sources*, 2010, **195**, 4727, DOI: 10.1016/j.jpowsour.2010.02.012.
258 L. Bi, E. Fabbri, Z. Sun and E. Traversa, *Energy Environ. Sci.*, 2011, **4**, 1352, DOI: 10.1039/C0EE00387E.
259 J. Xiao, W. Sun, Z. Zhu, Z. Tao and W. Liu, *Mater. Lett.*, 2012, **73**, 198, DOI: 10.1016/j.matlet.2012.01.032.

260 I. Luisetto, S. Licoccia, A. D'Epifanio, A. Sanson, E. Mercadelli and E. Di Bartolomeo, *J. Power Sources*, 2012, **220**, 280, DOI: 10.1016/j.jpowsour.2012.07.136.

261 H. Bae, J. Choi, K. J. Kim, D. Park and G. M. Choi, *Int. J. Hydrogen Energy*, 2015, **40**, 2775, DOI: 10.1016/j.ijhydene.2014.12.046.

262 Z. Zhu, W. Sun, Z. Shi and W. Liu, *J. Alloys Compd.*, 2016, **658**, 716, DOI: 10.1016/j.jallcom.2015.10.275.

263 J. Xiao, H. Yuan, L. Chen, C. Xiong, J. Ma, Y. Zhao, J. Chai, W. Du and X. Zhu, *Int. J. Mod. Phys. B*, 2017, **31**, 1744062, DOI: 10.1142/S0217979217440623.

264 Z. Zhu, S. Wang, J. Shen, X. Meng, Y. Cao, Z. Wang and Z. Wei, *J. Alloys Compd.*, 2019, **805**, 718, DOI: 10.1016/j.jallcom.2019.07.12.

265 Z. Sun, E. Fabbri, L. Bi and E. Traversa, *J. Am. Ceram. Soc.*, 2012, **95**, 627, DOI: 10.1111/j.1551-2916.2011.04795.x.

266 D. Pergolesi, E. Fabbri and E. Traversa, *Electrochem. Commun.*, 2010, **12**, 977, DOI: 10.1016/j.elecom.2010.05.005.

267 W. Sun, Z. Shi, M. Liu, L. Bi and W. Liu, *Adv. Funct. Mater.*, 2014, **24**, 5695, DOI: 10.1002/adfm.201401478.

268 Z. Zhu and S. Wang, *Ceram. Int.*, 2019, **45**, 19289, DOI: 10.1016/j.ceramint.2019.06.179.

269 S. Fop, *J. Mater. Chem. A*, 2021, **9**, 18836, DOI: 10.1039/D1TA03499E.

270 N. Tarasova and I. Animitsa, *Materials*, 2021, **15**, 114, DOI: 10.3390/ma15010114.

271 N. A. Tarasova, I. E. Animitsa, A. O. Galisheva and D. A. Medvedev, *Electrochem. Sci. Technol.*, 2022, **1**, 20221004, DOI: 10.15826/elmattech.2022.1.004.

272 E. P. Antonova, *Electrochem. Sci. Technol.*, 2023, **2**, 20232021, DOI: 10.15826/elmattech.2023.2.021.

273 A. P. Anantharaman and H. P. Dasari, *Ceram. Int.*, 2021, **47**, 4367, DOI: 10.1016/j.ceramint.2020.10.012.

274 B. Choudhary, L. Besra, S. Anwar and S. Anwar, *Int. J. Hydrogen Energy*, 2023, **48**, 28460, DOI: 10.1016/j.ijhydene.2023.03.393.